# Carbon footprint of solar based mini-grids in Africa: Drivers and levers for reduction

T. Chamarande, B. Hingray, Sandrine Mathy

# Carbon footprint of solar based mini-grids in Africa: drivers and levers for reduction

Chamarande, T.[1*], Hingray, B.[2], Mathy, S.[3]

[1]ESPACE-DEV, Univ Montpellier, IRD, Univ Antilles, Univ Guyane, Univ Réunion, 34 090 Montpellier, France
[2] Univ. Grenoble Alpes, CNRS, INRAE, IRD, Grenoble INP, IGE, 38000 Grenoble, France
[3] Univ. Grenoble Alpes, CNRS, INRAE, Grenoble INP, GAEL, 38000 Grenoble, France
[*]Corresponding author: theo.chamarande@ird.fr

## Abstract

The massive development of mini-grids (MGs) is seen as a promising alternative to the extension of national grids to achieve universal access to electricity. MGs based on solar photovoltaic are often recognized fully consistent with net-zero CO2 emissions objectives. However, if they have low or even no direct emissions from diesel consumption, they embed indirect carbon emissions due to solar panels and batteries manufacturing. Electrification policies, mainly based on the levelized costs of electricity (LCOE), should likely account for the carbon footprints (CFP) of possible electrification strategies.

In this work, we assess the CFP of hybrid MGs (solar, battery, diesel) for rural electrification in Africa. We consider a large number of MG configurations for many locations across the continent. For each location, we identify the lowest CFP and LCOE, and estimate their dependency to meteorological and socio-economic factors.

Our results show that: (i) the lowest CFP depends on location and is around 200gCO2/kWh; (ii) it can be higher than the CFP of certain African national grids; (iii) the CFP of hybrid MGs can be lower than the CFP of MGs relying only on solar PV; (iv) for most techno-economic and environmental assumptions, moderate LCOE increases allow significant CFP reductions.

**Keywords:** PV hybrid mini-grids, rural electrification, levelized cost of electricity (LCOE), carbon footprint, Africa

**List of abbreviations:**

- CF: Mean capacity factor of the solar production [-]
- CFP: Carbon footprint [$g_{CO2,eq}$/kWh]
- CFP*: Mini-grid configuration with the lowest carbon footprint
- DHI: Diffuse Horizontal Irradiance [W/m$^2$]
- DNI: Direct Normal Irradiance [W/m$^2$]
- GHG: Greenhouse Gases Emissions
- GHI: Global Horizontal Irradiance [W/m$^2$]
- GTI: Global Tilted Irradiance [W/m$^2$]
- LCOE: Levelized Cost of Energy [$/kWh]
- LCOE*: Mini-grid configuration with the lowest LCOE
- MG: Mini-grid
- NE: Nocturnal Energy consumption, mismatch indicator [kWh]
- PV: Photovoltaic
- SPC: Shadow price of carbon [$/$t_{CO2,eq}$]

- $\sigma_{diff}$: Mismatch indicator related to the daily difference in power between solar production and electricity demand [-]

# 1. Introduction

According to the International Energy Agency, more than 40% of the sub-Saharan African population does not have access to electricity [1]. Achieving Sustainable Development Goal 7, i.e., ensuring universal access to reliable, affordable, and sustainable energy by 2030, would require providing electricity to around 90 million more people on this subcontinent each year [2]. To reach this objective at the lowest cost, the International Energy Agency estimates that one third of these future electricity connections could be met by mini-grids (MGs), especially in remote areas, with the remaining two thirds relying on grid extension and solar home systems [1].

This electrification must be compatible with the objective of the Paris agreement to keep global warming below 2°C and as close as possible to 1.5°C [3]. Global pathways likely to limit warming to 2°C require net-zero CO2 emissions to be reached by 2070-80 (respectively as soon as 2050 for warming limited to 1.5°C). The power generation sector is the first that will have to be completely decarbonized [4]. Some African countries, like Namibia and Nigeria, have submitted very ambitious National Determined Contributions (NDCs) to the Paris Agreement aiming at net-zero emissions by 2050 and 2060 respectively [3]. A large literature focuses on how to reduce the greenhouse gases emissions (GHG) and achieve these NDCs with economic instruments such as carbon taxes [5-9], feed-in-tariffs [10, 11], subsidies on renewables installations [12, 13], green finance [14-17], clean development mechanisms [18], etc.

The NDC objectives only cover territorial emissions, i.e. direct emissions from households and emissions associated with production in the territory, but do not cover emissions linked to imports. However, these indirect emissions can represent very significant levels of emissions compared with local emissions [19]. For instance, the consumption-based emissions of the European Union are 65% higher than the territorial emissions [20]. This may have consequences for the policies required: a carbon border adjustment mechanisms (CBAM) has been recently adopted in Europe to target these embedded emissions from imported goods [21].

Many recent studies have pointed out the embedded emissions in the power sector. They especially demonstrated that renewable energy technologies [22] are not “equally low-carbon” [23]. For instance, the electricity production from solar PV do not emit any GHG, but solar PV comes with non-negligible indirect GHG emissions due to energy required for material extraction and for manufacturing of PV panels [24-27]. The notion of carbon footprint (CFP) was introduced and is used to estimate the amount of GHG emissions associated with all activities of a given entity. For the electricity production sector, it includes direct emissions required for energy production (e.g. fuel combustion), but also indirect emissions associated to supply chains and all energy transformations upstream (e.g. manufacturing, transport, distribution) and downstream (recycling, dismantling, etc.). The CFP of renewable energy technologies for instance depends on the electricity mix available for their production [28]; it is much larger if the mix is mainly based on fossil fuel than if it is based on renewable energy (hydropower, solar) and nuclear. The CFP also depends on the energy intensity of material extraction and of components manufacturing [29]. This depends on the efficiency of extraction / transformation processes and on material accessibility. The CFP could thus continuously increase in the next decades, as a result of the continuous decrease of ore concentrations in ore deposits worldwide due to the large amounts of materials and ores required for components manufacturing [30].

Many publications focus on the CFP of specific renewable energy technology (e.g., solar [31], wind [32], hydro [33], biomass [34]). Nevertheless, there is a need to go a step further and consider the CFP at a grid level. The massive introduction of renewable productions in the grid necessarily comes with the provision of a number of flexibility means to balance the intermittency of the production [35]. And the CFP of those flexibility means is not expected to be negligible. The needs for flexibility means is even more crucial for off-grid systems. Solar hybrid off-grid mini-grids, i.e. systems that are not connected to a national grid, have actually to deal with the solar resource variability at the local scale which may be large. As they can often not benefit from flexible renewable sources like hydropower, they typically need battery storage and/or diesel genset to deliver electricity in low resource periods. A fair estimate of the CFP of renewable energy technology should thus ideally also account for the CFP of the required flexibility means [27,36]. The CFP of 100% solar MGs in India and Africa was actually shown to highly depend on the PV/battery configuration and can be quite large [37,38].

MGs based on solar PV are promoted by international institutions as a "clean" solution to electrify rural areas worldwide with several hundred million US dollars invested in Africa each year in the last decade [39]. They indeed allow a large reduction of direct GHG emissions when replacing a diesel generator with solar PV and batteries in areas far from the grid [40,41]. Most of the studies assessing the GHG emissions of MGs however only consider direct GHG emissions [42-48] and conclude that replacing diesel generators with PV/battery MGs would completely cut GHG emissions [41,49]. Not taking indirect emissions into account however underestimates the GHG emissions associated with MGs. To evaluate the real impact of developing solar MGs on GHG emissions, one should not restrict the assessment to the MG direct emissions but should conversely consider the MG CFP [50].

A number of studies quantified the CFP of MGs for different locations in Tanzania [51], Greece [52], Rwanda [53], Italy [54], Alaska [55], Colombia [56], etc. The CFP can significantly vary from one location to the other, even at the country scale. These variations result from differences in the solar resources or from differences in technical / socioeconomic features of the considered systems [57]. To our knowledge, continental scale assessments of the CFP of MGs are lacking. Lu et al. estimated the CFP of PV production systems but which are grid-connected and thus they disregard the CFP of flexibility means [58]. A continental scale assessment would help policymakers to adapt their policies and electrification strategies.

Recent work to support policymaking primarily focuses on levelized costs of energy (LCOE). Many different MG configurations hybridizing solar PV, diesel gensets and batteries can supply the production required for a given community. As recent literature reviews have shown [59,60], most studies seek to identify the lowest cost MG configuration and to assess the corresponding LCOE [49, 61-65]. In planning studies at the regional level, this lowest LCOE configuration is typically compared to other rural electrification options (solar home systems, MGs, and grid extension) [66,67]. This is also the case in numerous studies dedicated to study cases for one or a few locations [60, 64, 66, 68].

The MG configuration with the lowest LCOE [53] is expected to differ from the MG configuration with the lowest CFP [69]. The LCOE of the former is expected to be smaller than the LCOE of the latter. Its CFP is conversely expected to be higher. The differences of LCOE and CFP between these two "optimal" configurations can be large but a variety of configurations are likely to provide reasonable trade-offs [70].

Our work explores the trade-offs between CFP and LCOE of solar based MGs for rural electrification in Africa, emphasizing the importance of including carbon footprint assessments in rural electrification policies, rather than focusing solely on cost minimization. It explores the socio-

economic and environmental drivers of CFP, possible levers for CFP reduction and possible trade-offs between CFP and LCOE minimization. For this, we specifically answer the following questions:

- What lowest CFP values can be achieved with hybrid MGs across Africa?
- How these CFP values differ from the CFP of other MG configurations, especially that of the lowest LCOE one or from the CFP of the national grids?
- What are the main technical, economic or environmental levers that can be used to lower the cost and/or the CFP of solar based MGs?
- What are the possible trade-offs between the lowest LCOE and lowest CFP MG configurations and are there trade-offs to achieve significant CFP reduction at low cost?

We first quantify the CFP and LCOE of a large number of MG configurations based on different solar/genset/storage setups for a large set of locations spread over the continent. The CFP and LCOE of each MG configuration is estimated from the simulation of the MG functioning over a full year period, which allows to account for the sub-daily to seasonal variability of both the solar resource and the demand (section 2). The simulations allow to identify the lowest CFP and LCOE configurations for each location, and then to assess how these configurations depend on both the characteristics of the resource and the demand. They also allow investigating different trade-offs between the lowest LCOE and the lowest CFP configurations and estimating the cost of different CFP reduction objectives (section 3). These results and their potential implications on future electrification policies are discussed in section 4.

The contributions to the literature are the following. First, we develop a generic and reproducible methodology to allow a continental scale assessment of the CFP of hybrid MGs. Second, we show that hybrid genset/solar MGs can achieve smaller CFP than 100% solar MGs. Third, we highlight that the CFP of MGs should be considered in environmental assessments instead of just direct GHG emissions and that it can be higher than the CFP of the national grid in some countries. Finally, we assess the LCOE increases required to achieve given CFP reduction levels in different climatic and socio-economic contexts, which will help designing policies towards net-zero carbon energy systems.

## 2. Methods

We considered fictitious hybrid MGs using solar PV, diesel gensets and batteries to supply typical load profiles for 93 different locations over Africa. We simulated the functioning of these MGs using meteorological data to estimate the solar resource and PV production, and simple dispatch rules for the use of the batteries and genset to ensure that supply always and fully meets electricity needs. Simulations cover a full year and are performed at a resolution of 15min to account for the sub-daily to seasonal variability of both the solar resource and the demand. Simulations are performed for a large range of configurations (PV panels and battery capacities). For each configuration, the LCOE and the CFP are estimated, allowing determining the configuration minimizing either the LCOE or the CFP.

The methodology, data and models are summarized in Figure 1 and are described in the following section and in Appendix A. All simulations and analyses are carried out using a script developed in Matlab© (script core available in Supplementary Material).

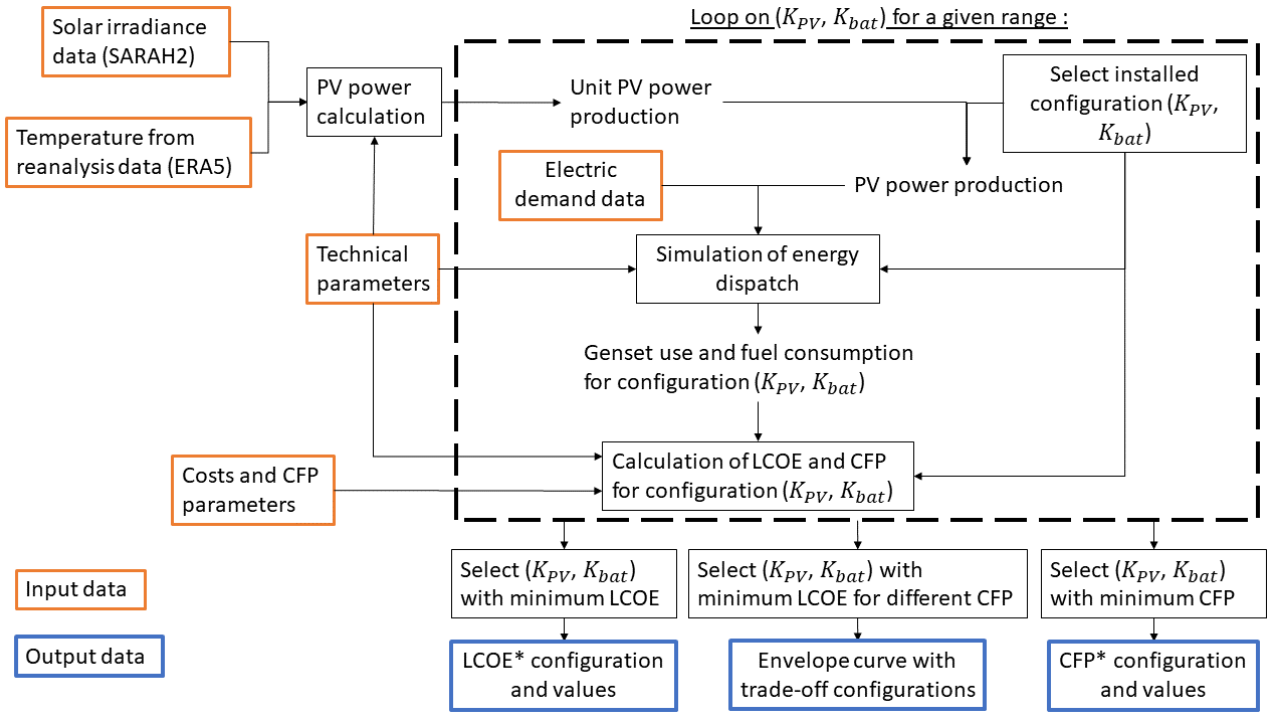


*Figure 1: Methodology of MG modelling. The calculation of PV capacity and electric demand data are specified in Appendix A. The loop on storage ($K_{bat}$) and PV ($K_{PV}$) installed capacities with energy dispatch and LCOE and CFP calculation are detailed in sections 2.1 and 2.2.*

## 2.1. MG modelling

To simulate the functioning of MGs, two time-series are required: a time-series of the load and a time-series of the production from renewable sources (only solar PV is considered here, but other sources like wind power could be added). In this study, the production time-series is estimated from time-series of local irradiance and local weather (extracted respectively from irradiance satellite products and global atmospheric reanalyses). The time-series of the load is constructed from load profiles taken from literature. Fifteen load profiles are used in this study to account for different seasonality and sub-daily patterns of the load. For the sake of simplicity however, most results presented next correspond to the so-called hybrid profile without seasonality. The load is assumed to result from a mix of productive and domestic uses and to be the same each day of the year. Details on data are given in Appendix A.

MGs considered in our work include a battery storage and a diesel genset. For our analyses, the functioning of a MG is simulated with a simple model based on the following assumptions and rules. The genset cannot be used to charge the batteries. The batteries can only be charged when solar PV production is higher than the demand. When solar PV production is higher than the demand and storage is full, the production is curtailed. When solar PV production is smaller than the demand, the residual demand can be satisfied with the genset, with the batteries or with both at the same time. The genset/battery energy dispatch rule is to maximize genset efficiency, i.e., the genset is used as closely as possible to its nominal power. This allows minimizing genset consumption. The battery is, therefore, used mainly during the lowest consumption hours. The battery efficiency for charge is assumed to be the same than for discharge: $\eta_{sto} = 0.95$.

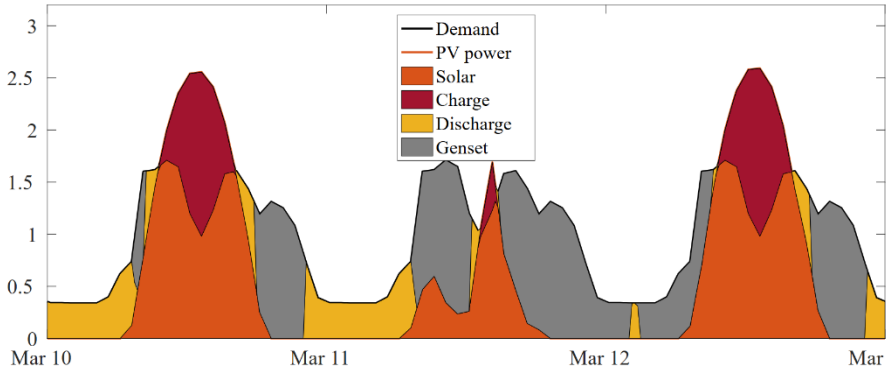


*Figure 2: Simulation of solar, genset and batteries dispatching for three days in March. The graph shows the simulation when maximizing genset efficiency. The y-axis corresponds to a normalized power: 1 corresponds to the mean power demand.*

The power to be produced by the genset for each time of the simulation period (Figure 2) allows estimating the total fuel consumption for the period, and in turn the direct emissions of the genset. More details on the genset consumption are given in Appendix A. To make sure that the electricity demand is always supplied, the genset installed capacity is set to the maximum value of the electric load profiles.

## 2.2. LCOE and CFP calculation and envelope curve

For a given configuration, namely for a given installed capacity of battery ($K_{bat}$ in [kWh]) and a given capacity of solar PV ($K_{PV}$ in [$kW_p$]), we simulate the functioning of the MG. This simulation allows to compute the diesel consumption required over the project lifetime to fully and always satisfy the electricity demand. The battery capacity $K_{bat}$, the PV capacity $K_{PV}$ and the diesel consumption allow to estimate the LCOE and CFP of the configuration. Equations as well as cost and carbon footprint parameters required for calculations are detailed in Appendix A, sections A.3 and A.4.

In the following, the LCOE and the CFP are estimated for a wide range of storage/PV capacity configurations. We consider storage capacities from 1hr•$\overline{D}$ to 20hr•$\overline{D}$ with $\overline{D}$ [kW] the mean power demand and solar PV capacities from 0 to 2.5$K_{PV}^0$, where $K_{PV}^0$ [kW] corresponds to the PV capacity that would be required to produce, over the one-year simulation period, an energy amount exactly equal to the total energy of a constant demand $\overline{D}$. In the following, the storage capacity is expressed in $[hrs_{eq}]$. One $hrs_{eq}$ corresponds to the energy required to satisfy one hour of the annual mean power demand $\overline{D}$. $K_{PV}^0$ is related to *CF*, the so-called mean capacity factor of PV panels as $K_{PV}^0 \cdot CF = \overline{D}$

To ease the comparison between sites, we use the normalized PV capacity defined by the ratio $K_{PV}/K_{PV}^0$, as shown in Figure 3. Two configurations are considered in the following: the LCOE* configuration that minimizes the LCOE, and the CFP* configuration that minimizes the CFP of the MG. These configurations are estimated by selecting, from the simulated configurations, the pair $(K_{bat}, K_{PV})$ with the minimum LCOE or CFP respectively.

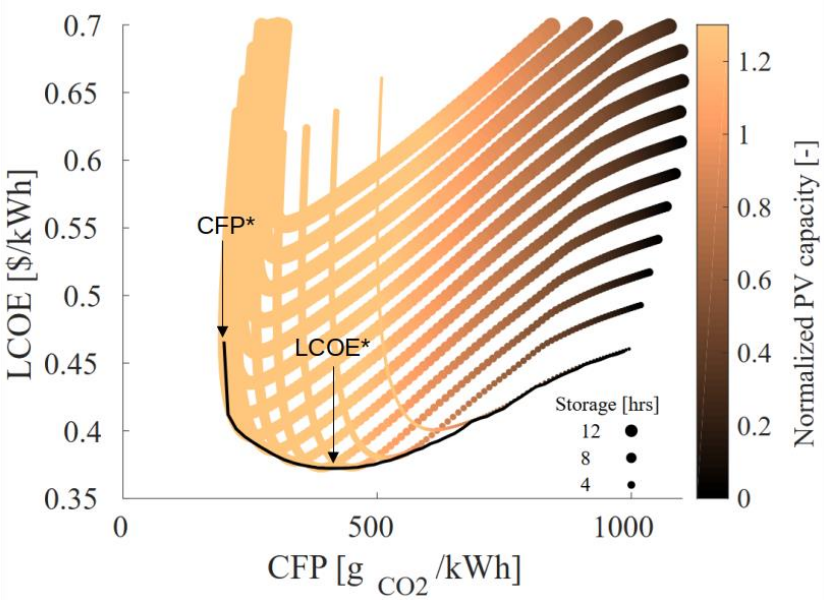


*Figure 3: Lowest LCOE (LCOE*) and lowest CFP (CFP*) configurations in a LCOE vs. CFP graph. The black line is the envelope curve. The colour shows the normalized PV capacity installed (dark dots refer to configurations with low penetration of solar, and light dots to high penetration of solar) while the size of the dots reflects the normalized storage capacity installed. Each U-shape line depicts a given storage capacity (only one out of three storage capacities simulated is represented). Each dot of each line corresponds to a given PV capacity. Each dot reflects a given genset production, i.e., the production required to satisfy the demand throughout the period. The storage capacity, the PV capacity and the genset production allow to estimate the CFP and the LCOE of the configuration. This graph is obtained for a location in Angola (-12.5°N; 17.5°E) with a hybrid load profile.*

The LCOE and CFP values obtained for all simulated PV capacity/storage configurations can be presented in a (CFP, LCOE) graph. As illustrated in Figure 3 for a given location, not all (LCOE, CFP) MG combinations are possible: it is not possible here to have a LCOE below 0.37 or a CFP below $200 g_{CO_2}/kWh$. In the remainder of the paper, the limit between the (LCOE, CFP) values that are possible and the ones that are not defines a so-called *envelope curve.* In practical, it is determined by selecting for each CFP value the lowest possible LCOE value.

This curve has two parts. The first goes from the diesel-only configuration to the LCOE* configuration. In this part, an increase in the PV capacity allows for a reduction in both the LCOE and the CFP. The second part joins both LCOE* and CFP* configurations, corresponding to the Pareto front between the LCOE and the CFP. This envelope curve shows the impact of the gradual integration of solar energy on LCOE and CFP.

# 3. Results

The first section shows the impact of considering CFP instead of focusing solely on direct GHG emissions. The second and third sections show the influence of the solar resource and its mismatch with electricity demand on CFP and LCOE values. The last section proposes different trade-offs between the CFP* and the LCOE* configurations. Most of the figures in this section illustrate the results for the mean values of technical, economic and environmental parameters. Other set of parameter values as well as other load profiles are additionally used to assess the robustness of our results (cf. figures in Appendix B).

## 3.1. Carbon footprint vs. direct GHG emissions of a mini-grid

We select one location in Angola (-12.5°N; 17.5°E) for illustration (green dot in Appendix A, Figure A.1), but similar results are obtained for other locations. To better understand the impact of

considering indirect emissions, Figure 4 shows for this location a comparison between the *envelope curve* including both direct and indirect emissions, and another *envelope curve* based only on direct emissions. This latter curve only considers GHG emissions produced by the genset consumption of diesel. It does not include the CFP from PV panels and batteries. When disregarding indirect emissions, a 100% solar system appears as a zero emission MG. Yet, indirect emissions are far from negligible. Even with a 100% solar system, they reach ~200gCO2/kWh, which is almost 20% of the CFP of a 100% genset MG configuration.

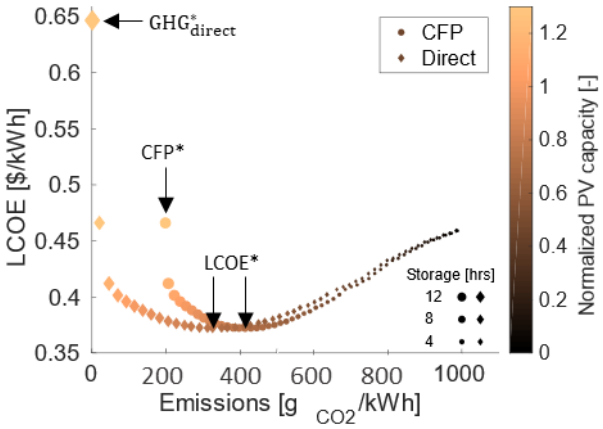


*Figure 4: Envelope curves reflecting CFP and direct emissions only for a location in Angola (-12.5°N; 17.5°E) with a hybrid load profile. Dots correspond to the whole CFP, including both direct and indirect emissions; diamonds depict direct GHG emissions only. The lowest CFP (CFP*), lowest $GHG_{direct}$ ($GHG^*_{direct}$) and lowest LCOE (LCOE*) configurations are indicated. Note that the LCOE* has the same (PV/storage/genset) configurations for both curves; only the level of GHG emissions differs.*

Figure 5 details the decomposition of the CFP into direct emissions from genset and indirect emissions induced by PV panels and storage. This decomposition is given for all configurations located between the economic optimum LCOE* and the carbon optimum CFP*. The LCOE* configuration corresponds to a solar penetration of 60% of the production mix, while indirect emissions from solar power represent 15% of the CFP. Moving from the LCOE* to the CFP* configuration along the curve in Figure 5 leads to an increase in the penetration rate of solar and in the capacity required for storage. The part of the CFP per kWh due to solar thus increases while the part due to genset decreases. Note that for high shares of solar in the mix, a part of the solar production is curtailed when the demand is satisfied and the storage is full. The solar share in the CFP is growing faster than its share in the energy supply because of this curtailement. The CFP* configuration thus corresponds to a compromise between lower diesel consumption and higher CFP due to higher solar and/or battery capacities. Hence, in the CFP* configuration, diesel is still used to supply a very small part of the energy (around 1% for this location, Appendix B Figure B.1).

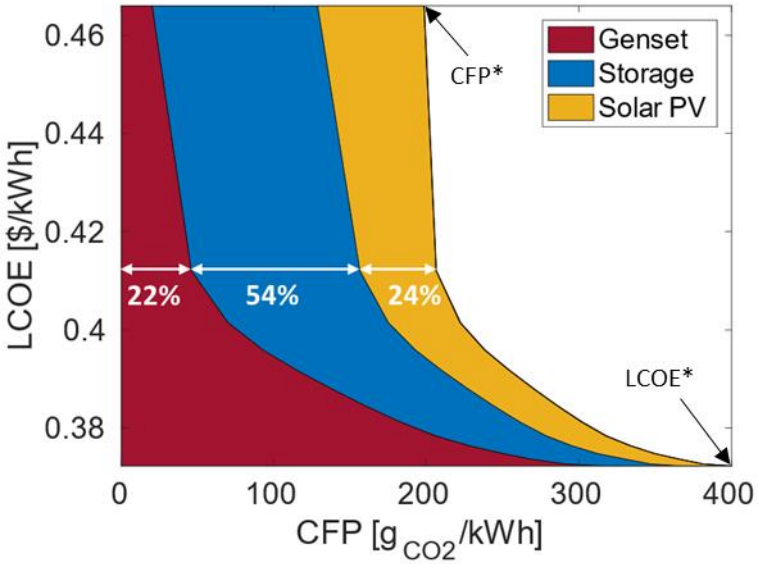


*Figure 5: CFP decomposition for a location in Angola (-12.5°N; 17.5°E) with a hybrid load profile for all configurations on the left-hand side of the envelope curve in Figure 4. The white arrows indicate how to read the graph: in this configuration LCOE = 0.415$/kWh and a CFP = 210gCO2/kWh, of which 22% is attributable to the genset, 54% to the batteries, and 24% to solar PV.*

This small part of diesel allows to fully supply the demand. A large part of the CFP of MGs is in fact due to the low resource days, those days requiring either large storage capacities or backup production means [71,72].

Reducing this part of diesel to approach a solar share close to 100% of the energy supplied can lead to a large increase of the CFP as it requires to install much larger battery capacities (Appendix B Figures B.2 and B.3). For instance, the lowest CFP of configurations with at least 99% (resp. 99.9%) solar production in the mix are up to 30% (resp. 50%) higher than the CFP of the CFP* configurations (cf. Appendix B Figure B.2).

## 3.2. The influence of solar resource on LCOE* and CFP* values

The LCOE* and CFP* values vary across the African continent (Figure 6) with similar spatial patterns. Regions far from the equator (Maghreb and the east coast of South Africa) and regions in Central Africa have higher LCOE* (~0.43$/kWh) and CFP* (~230$g_{CO2}$/kWh) than other regions. In the Sahara for instance, LCOE* values are around 0.35$/kWh and CFP* approximately 190$g_{CO2}$/kWh. For comparison, the genset-only configuration has a CFP equal to 996 $g_{CO2}$/kWh and a LCOE equal to 0.46$/kWh.

In almost all cases, when compared to a genset-only configuration, CFP* configurations lead to a large CFP reduction, at least 75%. Note that LCOE* configurations, which result in a 15% LCOE reduction, already lead to a significant CFP reduction, from 50 to 65% (Appendix B Figure B.4).

For the CFP* configurations, whatever the region, the genset is still required to supply a low but significant percentage of the energy, up to 6-8% in some specific locations (Figure 6, bottom). The renewable fraction, i.e., the percentage of energy supplied by solar PV (or batteries), is high (from 92% to 99%). For the LCOE* configurations, the genset has a much higher contribution (from 20% to 50%), and the renewable fraction is much lower (from 50% to almost 80%). These LCOE values are in the upper range of what can be found in the literature as we consider mean current values of costs without including potential costs decrease in the future. Regarding the CFP values, our estimates are rather similar to what was already presented in the literature [54, 56, 73]. The same applies for the renewable fractions obtained for the LCOE* configuration.

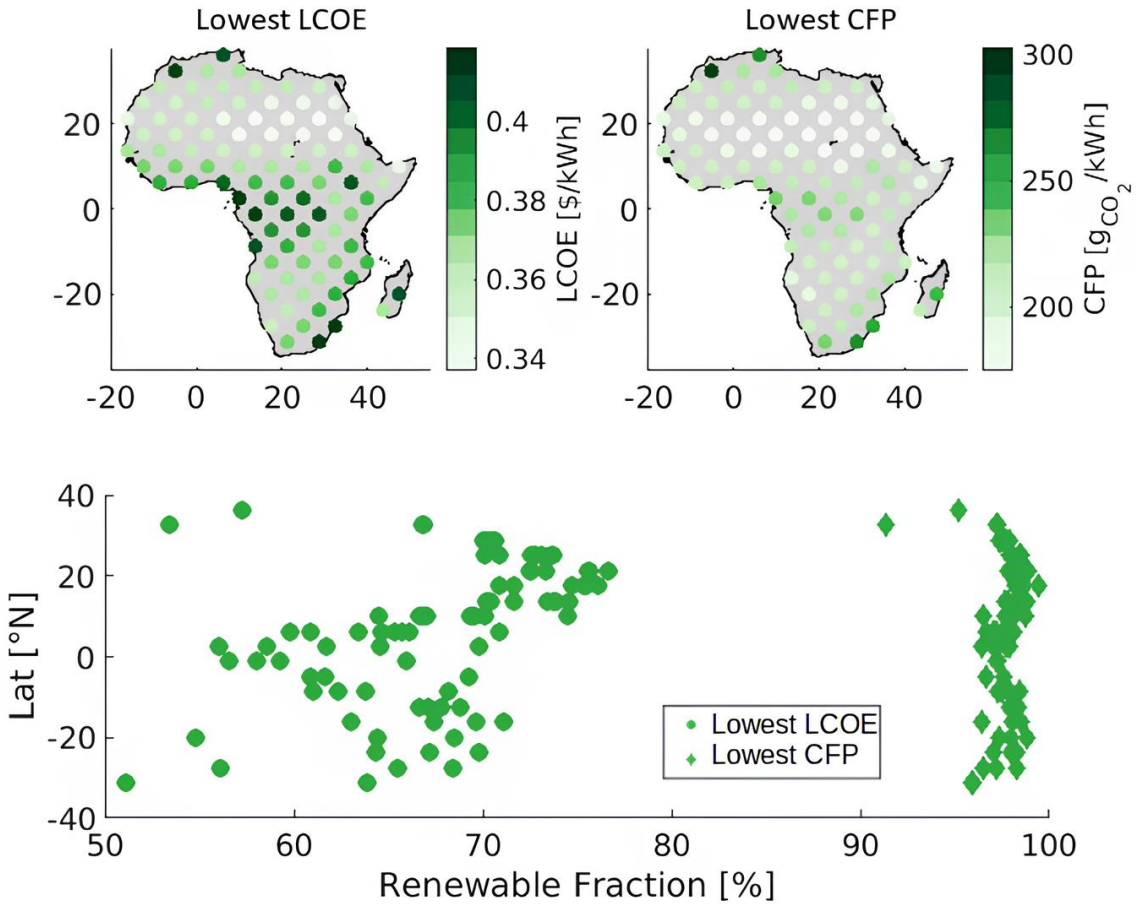


*Figure 6: Lowest LCOE (top left) and lowest CFP (top right) for all locations with a hybrid load profile. LCOE and CFP for a diesel-only configuration are respectively equal to 0.46$/kWh and 996g$_{CO2}$/kWh. The renewable fraction (bottom chart) corresponds to the proportion of the energy demand supplied by solar and batteries.*

The LCOE* and CFP* values and configurations are expected to depend on the characteristics of the resource and on its temporal adequation with the load. For illustration, the CFP* and LCOE* values obtained for the 93 locations and 15 load temporal profiles are presented as functions of different variables in Figure 7: CF, $\sigma_{diff}$ and NE. CF corresponds to the mean annual solar resource,expressed with the annual capacity factor. $\sigma_{diff}$ is the day-to-day resource/demand mismatch and it is computed as the standard deviation of the day-to-day resource /demand difference (cf. Appendix A, section A.2) [74]. N.E. is the the so-called nocturnal energy (N.E.), a measure of the fraction of the daily energy to be satisfied each day at night when the solar resource has gone (cf. Appendix A, section A.2) [74].

Both CFP* and LCOE* values are significantly correlated to these three variables. CFP* and LCOE* are higher when the mean annual resource is lower, when the day-to-day resource/demand mismatch is higher or when the nocturnal energy is higher. The correlation is very high with the nocturnal energy (0.97 for CFP*; 0.89 for LCOE*), much lower but still important with the day-to-day mismatch (0.39 for CFP* and 0.49 for LCOE*) or with the capacity factor (-0.22 for CFP* and -0.39 for LCOE*). The most impacting factors for both CFP* and LCOE* are thus related to the mismatch between the resource and the demand. The important mismatch features are first related to the sub-daily profile of the demand, which determines the amount of storage required to shift part of the within day solar production to evening or night hours. They next correspond to the day-to-day resource/demand adequation, which depends on both the mismatch of seasonal variations and on the meteorological variability of the resource. These day-to-day variability leads to low-resource days of potentially high impact for the system as explained in [71, 74]. In our context, CFP* and LCOE* are for instance globally much smaller when the demand has no seasonality (a demand without seasonality makes here the day-to-day mismatch much lower for most locations (see the $\sigma_{diff}$ axis of Figure 7).

As shown in the supplementary material, these results are robust and do not depend on the socio-economic and environmental assumptions required for calculations (Appendix B, Figures B.5).

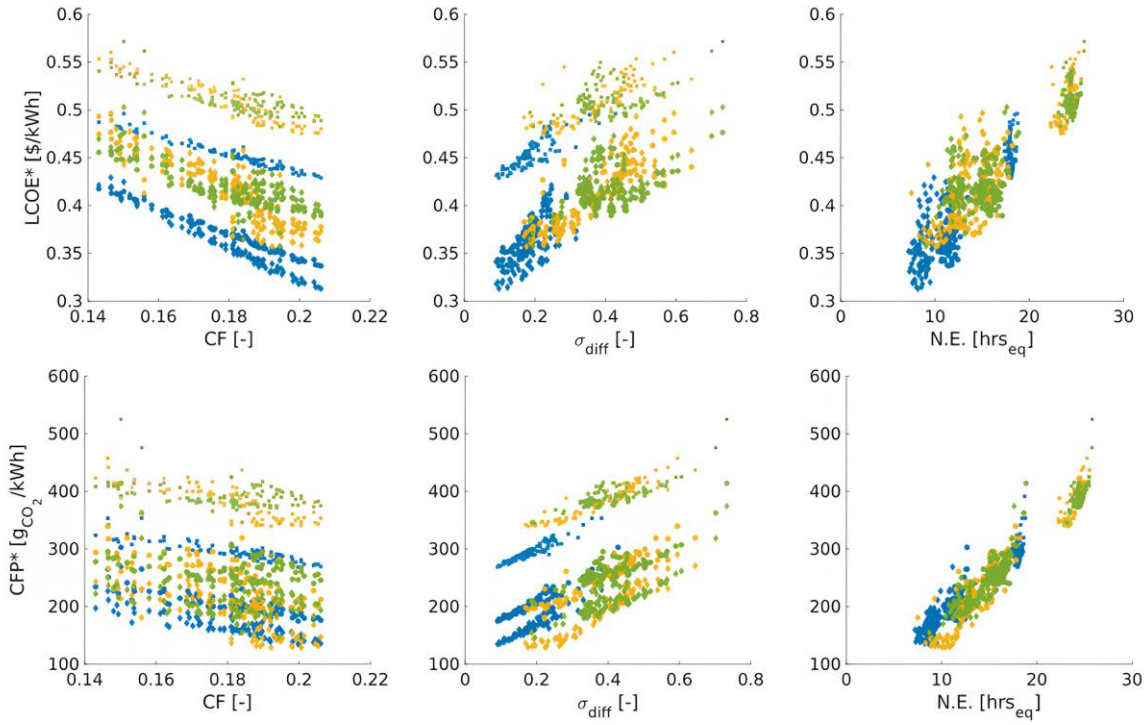


*Figure 7: Lowest LCOE (top) and lowest CFP (bottom) for all locations and 9 demand profiles as a function of the mean capacity factor (CF) (left), the day-to-day mismatch ($\sigma_{diff}$) (middle) and the nocturnal energy (right). The colour corresponds to a seasonality (blue: no seasonality; for other colours, the demand is seasonal with the highest demand in June and December for yellow and green respectively). Different markers account for different sub-daily load profiles: squares for domestic, circles for hybrid and diamonds for productive.*

## 3.3. Distance between the LCOE* and CFP* configurations

The distance between the LCOE* and the CFP* configurations depends on location and on the demand profile. It also significantly depends on the resource/demand mismatch features (Figure 8). Switching from LCOE* to CFP* configuration allows for a reduction of 20% to 60% of the CFP but at the cost of an increase in LCOE of between 10% and 70%. In sites with a higher mean capacity factor and lower mismatch ($\sigma_{diff}$ and N.E.), the LCOE* configuration is closest to the CFP* configuration. In sites with a lower mean capacity factor, the distance between both configurations is greater, leading to higher CFP reduction potential.

For locations with similar mean capacity factor, a higher mismatch leads to relative changes that are larger in LCOE and smaller in CFP. The locations with higher mismatch are typically located far from the equator. Their solar resource has a greater seasonality, which requires increased PV capacity to deal with periods of low solar resource.

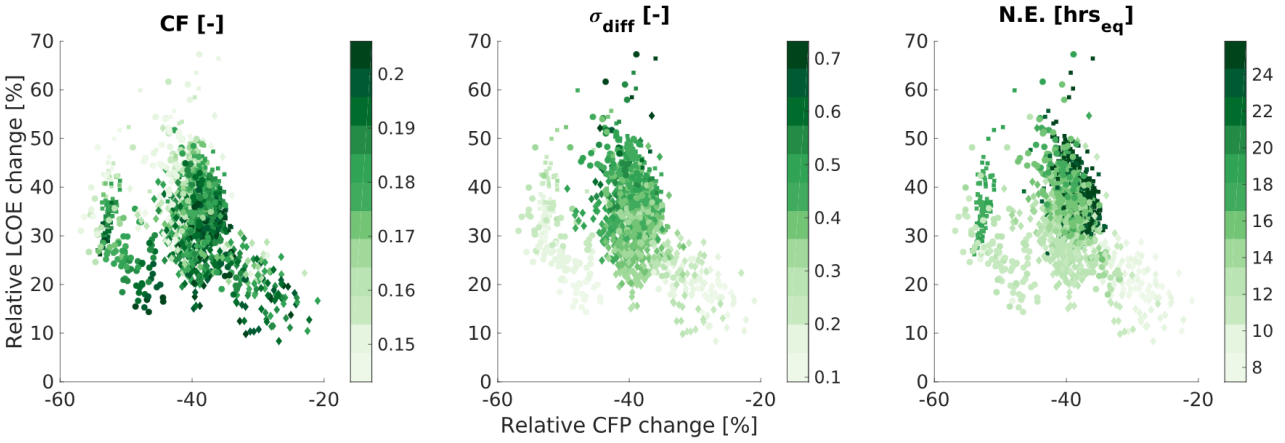


*Figure 8: Relative changes between the LCOE* and the CFP* configuration. The relative CFP change (resp. LCOE change) corresponds to a CFP reduction (resp. LCOE increase) obtained from the LCOE* configuration to the CFP* configuration. The dark colour indicates a higher value of mean capacity factor (left), of the day-to-day mismatch indicator ($\sigma_{diff}$, middle) and of the nocturnal energy (right) while the lighter green shows lower value for these variables. Different markers account for different sub-daily load profiles: squares for domestic, circles for hybrid and diamonds for productive.*

The increase in LCOE required to move from the LCOE* to the CFP* configuration is over 20% in most cases. This increase can be considered prohibitive in the context of rural electrification, as the local population cannot afford high electricity tariffs. However, many other MG configurations can serve as trade-offs between the CFP* and the LCOE* configurations.

## 3.4. The possibility for trade-off configurations between LCOE* and CFP*

The distance between LCOE* and CFP* configurations can be rather large, making the promotion of CFP* configurations rather unrealistic. Trade-off configurations could present more reachable targets.

Looking at Figure 9, the slope of the *envelope curve* for different locations on a North-South transect (blue dots in Appendix A, Figure A.1) is very steep near the CFP* configuration. Near this point, substantial LCOE increases are required to achieve only small CFP reductions. Conversely, the slope is slight around the LCOE* configuration. The shape obtained for these curves (i.e., a slight linear decrease of costs when integrating renewable followed by a large increase for very high renewable fraction) is very similar to previous works carried out for specific case studies [56, 73, 75] or for national grids [76]. Near the LCOE* point, significant CFP reductions can be obtained with low or moderate LCOE increases.

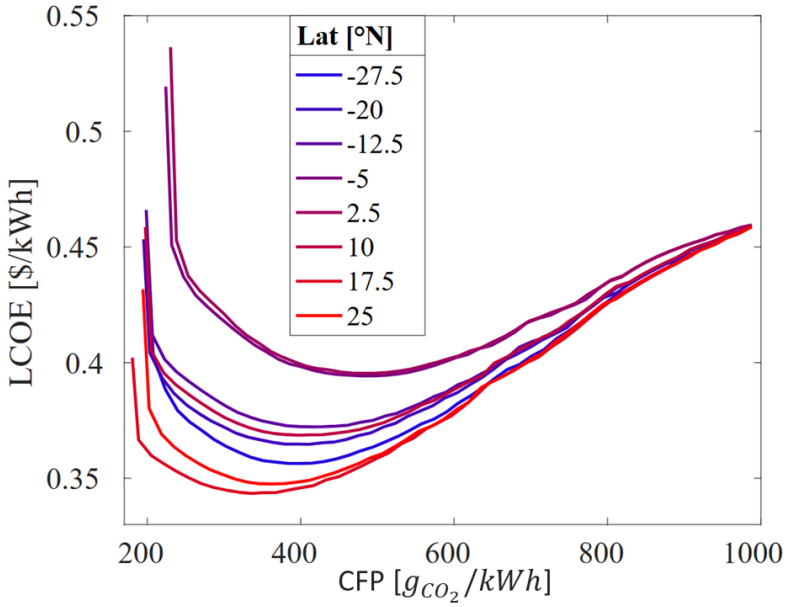

*Figure 9: Envelope curves for the N-S transect locations (Longitude 17.5°E, blue dots in Appendix A, Figure A.1). Each curve represents a different latitude: red for the northernmost location of the transect and blue for the southernmost.*

This highlights the potential for significant reductions of the CFP of MGs with only moderate additional costs compared to the lowest cost configuration. Figure 10 shows the reduction in CFP from the LCOE* configurations that can be achieved for the 93 locations with different predefined levels of LCOE increase (Figure 10 left), and, from another point of view, the increase in LCOE needed to achieve different predefined levels of CFP reduction (Figure 10 right).

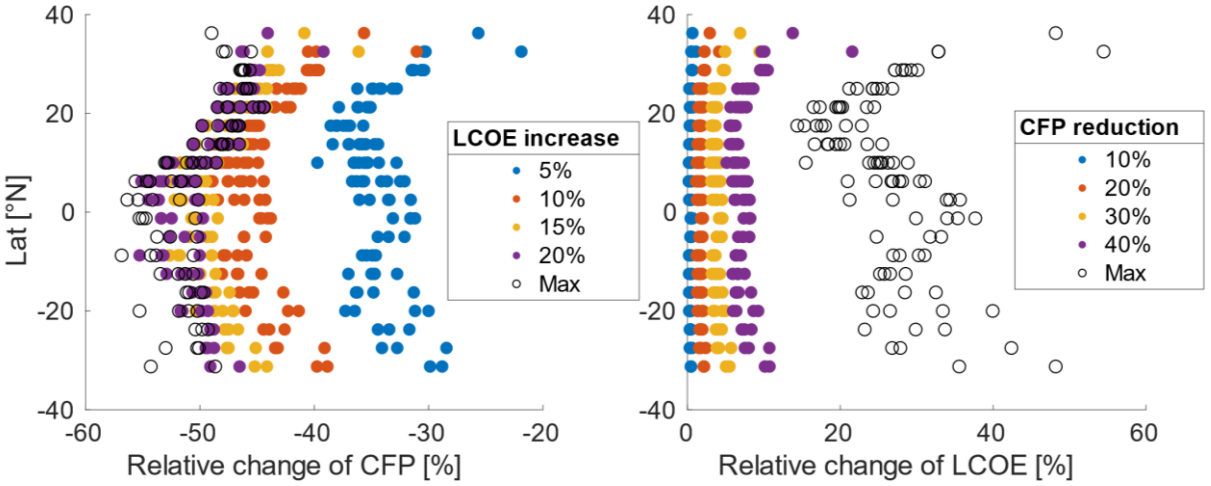


*Figure 10: Left: Reduction of the CFP from the LCOE* configuration with different levels of LCOE increase. Right: Increase in LCOE from the LCOE* configuration for different objectives of CFP reduction. In both graphs, "Max" corresponds to the relative changes in CFP and LCOE obtained with the CFP* configurations.*

The CFP reduction achieved with only a 5% (resp. 10%) increase in the lowest LCOE value is between 25% and 40% (resp. 40% to 50%) in most locations. A 20% increase in the LCOE allows lowest CFP values to be reached in many locations, with some exceptions far from the equator and in Central Africa (in the equatorial zone). Relative changes in LCOE to achieve 30% CFP reduction are much lower (<10%) and less sensitive to latitude than those required to reach the lowest CFP values (17%-50%).

These results depend on the techno-economic and CFP assumptions retained for the analysis. Values of CFP, costs and lifetime are highly variable depending on the installation and the components chosen [27]. For instance, the cost of fuel in Nigeria is around 0.6$/L, whereas it is approximately 1.3$/L in Rwanda [77]. The CFP of a $kW_p$ of PV produced with a decarbonized electricity mix is half that produced with an electricity mix with a high proportion of coal [29]. The socio-economic context modifies the shape of the envelope curves (Appendix B, Figures B.6 and B.7), and thus, the level of CFP reduction that can be achieved with moderate additional costs. Our simulations performed with many different scenarios of cost, CFP and lifetime assumptions (Appendix A, section A.5) tend to slightly modify the high level of CFP reductions obtained here.

Among the different scenarios simulated, a 10% LCOE increase leads to a CFP reduction of over 40% in only 20% of cases (Appendix B Figure B.8). This lower CFP reduction is partly due to a lower CFP distance between LCOE* and CFP* configurations that limits the possibility of emission reductions. The number of cases where the CFP reduction is over 40% almost double when removing the cases where this CFP distance is below 40% (Appendix B Table B.1).

Our method allows to identify the set of socio-economic and environmental contexts for which it is the most difficult to achieve significant CFP reduction. Low CFP reductions are mostly the result of a low fuel cost (Appendix B, Figure B.9) when combined with other factors (e.g., high cost of solar PV and batteries, load profile without seasonality; Appendix B, Tables B2 and B.3).

All in all, a significant CFP reduction can be obtained with moderate additional costs in most cases. When this is not the case, it is typically because the CFP distance between the LCOE* and CFP* configurations is already small or because a combination of socio-economic factors strongly disadvantages the use of solar PV and batteries.

# 4. Discussion and policy implications

## 4.1. Potential levers to reduce the CFP and LCOE of MGs

As explained in the methodology (cf. section 2), simulations have been performed for a large set of CFP, costs and lifetimes assumptions allowing us to explore the sensitivity of LCOE and CFP values to these different parameters. More details on this global sensitivity analysis are given in Appendix A [78].

The sensitivity of CFP (resp. LCOE) to a given parameter X is estimated from the relative slope of the function CFP(X) (resp. LCOE(X)) when only this parameter X is modified. For instance, a 0.3 sensitivity value for CFP* to X means that the value of CFP* increases by 30% if X increases by 100%. One value of sensitivity is computed for each scenario of location, demand profile, discount rate and parameters related to components (cost, CFP, and lifetime), resulting in distributions of the sensitivity values associated to each parameter (Appendix A). These distributions are summarized for the LCOE and for the CFP of the CFP* and LCOE* configurations in Figure 11.

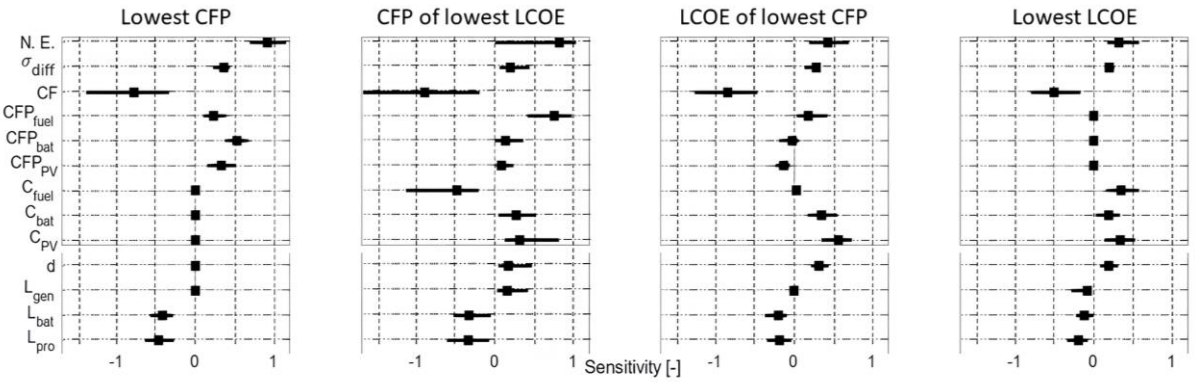


*Figure 11: Distribution of LCOE and CFP sensitivities to each parameter for LCOE* and CFP* configurations. The lines correspond to the distribution between the 10th and 90th percentile; the square is the value of the median. For sensitivity related to locations and load profiles, three variables were computed to characterize the variations in solar resource and in the mismatch of this resource and power demand: the mean capacity factor, the first mismatch indicator $\sigma_{diff}$ and the nocturnal energy (Appendix A). Results were obtained for the 8 locations on the North-South transect (blue dots in Appendix A, Figure A.1).*

The results of this sensitivity analysis allow to study the robustness of results, but also to identify the levers on which public policies can act to reduce the LCOE and CFP of MGs.

As shown in section 3.2, LCOE and CFP values are very sensitive to the solar resource and its mismatch with the electric demand (CF, day-to-day mismatch and NE). However, it is not possible to modify the solar resource and it is difficult to deeply modify the load profile even with demand-side management.

If we consider that MG developers usually supply electricity at the lowest cost [79-81], policies should first focus on the reduction of CFP and LCOE for the LCOE* configuration. These CFP and LCOE values are especially sensitive to the fuel cost, but with opposite effects. Subsidizing the fuel

cost would decrease the LCOE but increase the CFP and vice versa. On the contrary, subsidizing solar PV allows to decrease both the LCOE and the CFP. The efficiency is a bit lower but still higher than subsidies on batteries for both the LCOE and the CFP.

Reducing the CFP of PV panels and batteries would have a relatively low impact on the CFP of the LCOE* configuration. This would conversely have a high impact on CFP* values, especially when reducing the CFP of batteries. However, PV panels and batteries are to date produced out of Africa, making African countries dependent on decarbonization policies chosen elsewhere. One lever would be favouring the importation of MG equipment from producers with low carbon electricity. This would however be likely accompanied with significant cost increase. Another lever for African countries with low carbon electricity mix (e.g., Ethiopia, Zambia [82]) would be to develop their own local productions.

The CFP and LCOE are less sensitive to the other parameters considered here. However, some of these parameters have a large range of variations which may lead to relatively large changes of the LCOE and the CFP. As an example, the LCOE and CFP sensitivities to battery lifetime or discount rate are relatively small but battery lifetime fluctuates from 2 to 10 years (x5) (due to maintenance, temperature, humidity conditions or overuse [83]), and the discount rate varies by 8% to over 30% (x4) (due to funding type or risk level [84]).

Policies should especially focus on the MG longevity. Whatever the MG configuration, increasing the project and battery lifetimes for instance can significantly decrease both the CFP and LCOE of MGs. Increasing MG longevity requires the development of technologies that are more robust to the African temperature and humidity conditions. This also requires extensive capacity building and improved governance to reach efficient maintenance as well as sustainable operation and development of the systems [85-88].

## 4.2. Estimating the cost of a CFP reduction policy

The previous sensitivity analysis highlighted the LCOE* and CFP* impacts of modifying technical, environmental or economic parameters. However, it does not inform on the economic efficiency of possible policies. As the financial resources for rural electrification and climate change reduction can be very limited in Sub-Saharan countries, investment should be prioritized. Looking at the economic efficiency of climate mitigation projects (i.e., how much it costs to avoid a ton of $CO_2$) allow to select the most economically relevant investments. This section illustrates how to estimate the economic efficiency of a CFP reduction through the concept of the shadow price of carbon (SPC).

This investment analysis method puts a virtual cost on the carbon emissions related to a project. This means that projects are penalised according to their GHG emissions. This approach is now a corporate commitment for all IBRD/IDA investment projects that are subject to GHG accounting *(IBRD: International Bank for Reconstruction and Development, IDA: International Development Association)* [89].

We estimate the shadow price of carbon required to move the LCOE* configurations to lower CFP configurations. It is defined as the carbon price that would have to be charged for direct and indirect emissions to ensure that the CFP* configuration, or any other configuration that reduces the CFP by a certain level (determined a priori) compared to the LCOE* configuration, minimizes the LCOE.

This is achieved by introducing into the LCOE calculation equation (Appendix A, section A.4) a shadow carbon price (*SPC* [$\$/t_{CO_2,eq}$]) on the diesel consumption and on the CFP of the different components (equation 1). The updated LCOE, to be minimized, then reads as follows:

$$LCOE_{SPC} = LCOE + CFP * SPC \quad (1)$$

Figure 12 shows the values of the SPC corresponding to specific levels of CFP reductions. The shadow carbon prices needed to move from the LCOE* to the CFP* configuration are exorbitant, reaching several thousand $\$/t_{CO_2,eq}$ (Figure 12 left). To give orders of magnitude, to limit warming to 2°C, the SPC for 2030 estimated by the IPCC (2022) would need to be between 60$\$/t_{CO_2,eq}$ and 120 $\$/t_{CO_2,eq}$. To limit warming to 1.5°C, it would have to be around 170-290$\$/t_{CO_2,eq}$ [4].

For the MG context considered here, smaller but still significant CFP reductions are achievable with these smaller shadow prices. For instance, a shadow price of 120 $\$/t_{CO_2,eq}$ is sufficient to reduce the CFP of the LCOE* configuration by more than 10% and, at 290$\$/t_{CO_2,eq}$, this reduction reaches between 30% and 40% (Figure 12 right, Appendix B, Figure B.10). Similar but smaller values are already in use: the European Investment Bank has used a SPC of 80$\$/t_{CO_2,eq}$ for energy projects in Senegal and Kenya in 2020 [90].

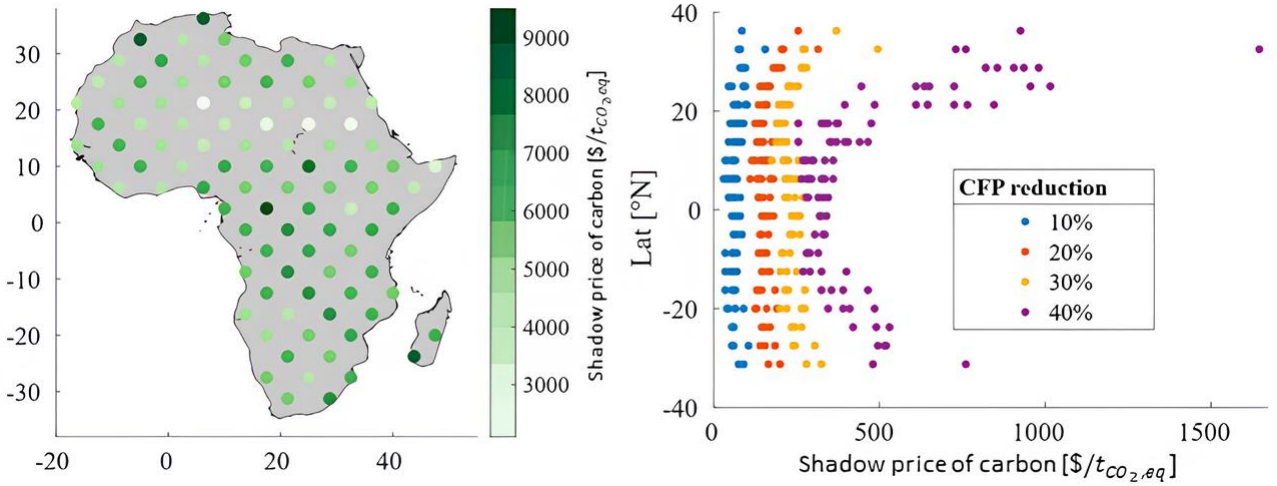


*Figure 12: Left, map of SPC (shadow price of carbon) required to go from LCOE* to CFP*. Right, value of SPC for all locations and for different objectives of CFP reduction. Both graphs are obtained with a hybrid load profile and using the reference values for all parameters.*

Note that the high SPC estimates obtained in our work were obtained including the indirect emissions in the scope of the carbon price, whereas World Bank estimates, as many others funding agencies or institutions, only consider direct GHG emissions. In our configuration, when considering only direct emissions, the SPC values required to go from the LCOE* to the CFP* configurations are divided by 2 to 4 (Appendix B Figure B.11). Achieving a real carbon neutrality at the global scale requires to consider the whole carbon footprint of energy systems in the design of policy, and the development of carbon border adjustment mechanism as in Europe shows the importance to know the indirect emissions embedded in energy technologies.

## 4.3. Grid vs. MGs from a CFP point of view

Planning studies presented for rural electrification have usually considered the lowest cost option between the development of MGs and that of the main national grid. They usually neglect GHG emissions. These studies indeed consider that MGs based on renewables are emissions-free, and thus, that they are better than the national grid on this aspect. However, including the CFP into this comparison would make this analysis less straightforward. The CFP of the main national grid may indeed be lower than the CFP* values of MGs for certain countries (Figure 13). This would be the

case for almost one fourth of the 93 locations studied in this paper, mostly located in countries with high hydropower potential such as Ethiopia or Democratic Republic of Congo.

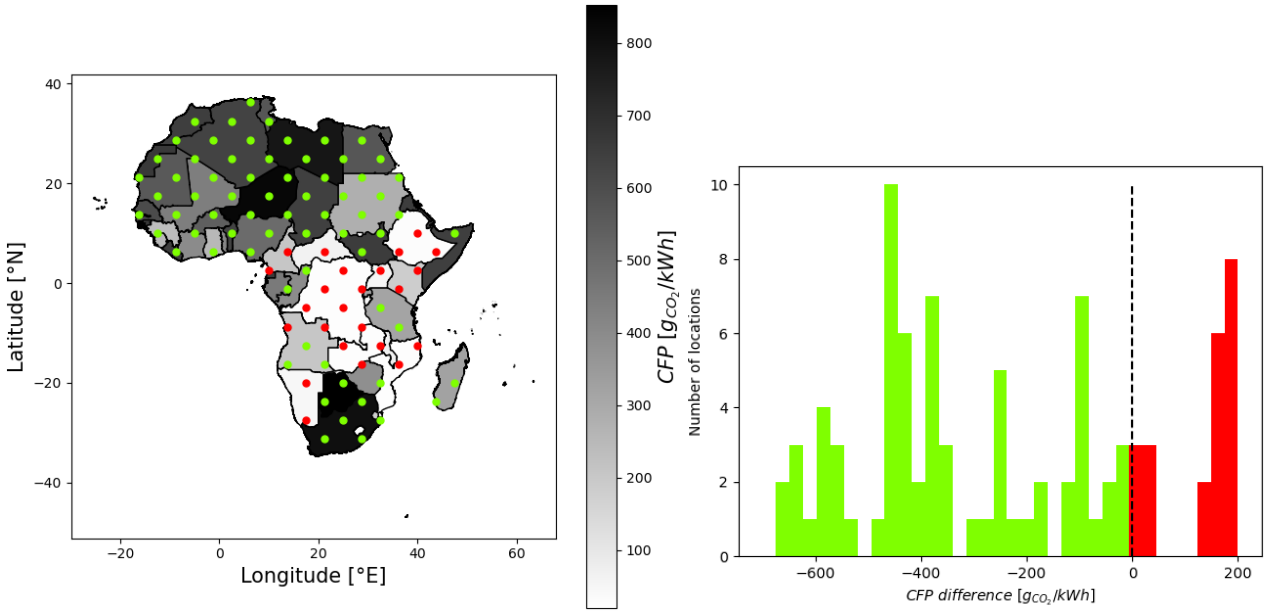


*Figure 13. Comparison of the CFP of MGs and of the national grid. Green dots (left) and bars (right) correspond to locations where MG CFP is lower than grid CFP. Red ones correspond to locations where MG CFP is higher than grid CFP. The black and white scale corresponds to the median of the grid CFP on the last 30 years extracted from [82].*

The comparison between the CFP of national grids and of MGs should also considered the geographical distribution of people without electricity. The largest potential for MG development can be found in countries with a low electrification rate, a large population growth and rural areas with growing energy demand for productive uses (e.g., mining, forestry) [1]. However, the CFP of national grid is lower than or close to the CFP of MGs in many of these countries (e.g., Democratic Republic of Congo, Ethiopia, Uganda). On the contrary, countries like South Africa, Algeria or Morocco where the CFP of national grid is high (cf. Figure 13) have a lower potential for MG development as their electrification rates are high, and their population and economy are growing slower than in Sub-Saharan Africa.

As Figure 13 does not include the carbon footprint related to the grid extension, it has to be treated with caution. Moreover, the data related to the CFP of national grids need to be consolidated. But this first step in the analysis shows that the CFP of MGs cannot be neglected.

The CFP of national grids may also be strongly modified in the next years depending on the resources available in each country and on the vision of the energy mix supported by policymakers [1]. In a scenario where fossil fuels are developed (e.g., oil in Uganda, gas in Senegal), the CFP of national grid could increase and become much higher than the CFP of MGs. The reverse could occur if renewables (hydropower in west and central Africa, wind in South Africa and/or solar) and/or international connexions (e.g., West African Power Pool) were actively developed. To a lesser extent, the CFP of MGs could also be reduced, for instance by developing MGs that combine multiple sources of energy (e.g., wind power, biomass) to produce energy from other renewable sources in low resource days.

## 5. Conclusion

The recent literature on MGs shows that renewable energies are still considered to be GHG emission-free, but they are not if indirect emissions are taken into account. Our work highlights that including

indirect emissions, MGs could have a higher CFP than national grids. To truly achieve carbon neutrality and be consistent with the Paris Agreements, policy makers need to take into account the CFP of the different electrification strategies and not only direct emissions.

We show that indirect emissions of PV panels and batteries have a non-negligible contribution to the CFP of MGs with high shares of solar production. They represent 15% of the CFP in systems where 60% of the demand is supplied by solar energy. Indirect emissions prevent the CFP from going below a certain CFP threshold. In the configurations that achieve the lowest CFP values, part of the CFP is due to the genset consumption (between <1% and 8% of supplied energy) still required to fix some low-solar resource periods.

In Africa, with the current mean costs, lifetimes, and CFP values of the different MG components, this lowest achievable CFP value varies from $180\ g_{CO_2,eq}/kWh$ to $250\ g_{CO_2,eq}/kWh$ for a hybrid load profile, depending on the location. Beyond the energy efficiency and the energy mix used for the extraction of materials, manufacturing processes and disposal of solar PV and batteries, the lowest achievable CFP values for MGs depend on the mean solar resource and of the mismatch between the resource and the electricity demand. Regions with a lower solar resource (e.g. Central Africa) or with a higher resource seasonality (Maghreb, South Mozambique) will have more difficulty to lower the CFP of MGs than regions with all the year abundant resource (e.g. Sahelian region).

When compared to a genset-only configuration, the lowest LCOE configuration allows for a decrease in both the LCOE (by around 15%) and the CFP (by more than 50%) of the MG. Moving further to the lowest CFP configuration increases the LCOE (often >20%) which may be an issue considering the scant ability to pay of many rural communities in Africa. However, smaller LCOE increases allow for significant CFP reductions. In many cases, a 5% LCOE increase is enough to reduce the CFP of the lowest LCOE configuration by more than 25%, and a 10% LCOE increase by more than 40%.

These results inevitably depend on several factors, such as the electricity demand profile, costs, CFP, and lifetimes of each MG component. Special attention should be paid to parameters with high impacts and high uncertainties, such as the electric load profiles [91-93], or the batteries and project lifetimes that have sometimes been observed at below two [83, 94] and six years [85,86] respectively. The results are also sensitive to the discount rate, which varies greatly depending on project risks and the profitability expected by the investors [84]. Policies could thus focus on how to decrease risks related to MG projects and how to improve the longevity of MGs to reduce both their CFP and their LCOE.

According to the International Energy Agency [95], MGs are expected to supply 160TWh in 2040. A 20% reduction in the CFP of future installed systems would lead to more than $13 Mt_{CO_2,eq}$ avoided each year, more than the yearly GHG emissions of a country such as Gabon (excluding land use change) [96]. Such estimates, although rough, show how important it is to guide MG developers toward low CFP configurations using incentives or a regulatory framework. These issues call for more research to design suitable policies.

The methodology we presented for estimating the CFP of MGs is rather generic and it could be easily applied elsewhere or extended to other MG configurations with other energy sources such as wind, hydro, biomass or other load scenarios. It can next be easily integrated in future research and / or decision support tools related to electrification planning. The methodology could be also extended to account for other design criteria, such as environmental ones. For instance, the use of diesel may have other environmental and health impacts (e.g., air and soil pollution, resources depletion [97,98]). Disposal of batteries and other electronic equipment may also lead to soil and water contamination [99]. The focus on GHG emissions chosen for this study could be extended to account for these other environmental impacts.

**Author Contributions:** conceptualization and methodology: T.C., B.H. and S.M.; software, formal analysis, writing - original draft preparation: T.C.; writing – review and editing T.C., B.H. and S.M.

**Conflict of Interest:** The authors declare no conflict of interest.

**Acknowledgements:** This work is part of a PhD thesis funded by the French Ministry of Higher Education, Research, and Innovation, and by Schneider Electric.

# Appendix A. Methodology

## A.1 PV production

The solar PV production is estimated at 15-minute resolution using global horizontal irradiance (GHI) from Heliosat SARAH 2 [100] and the air temperature from ERA5 reanalysis [101]. These data are collected for 93 locations over two years (Figure A.1).

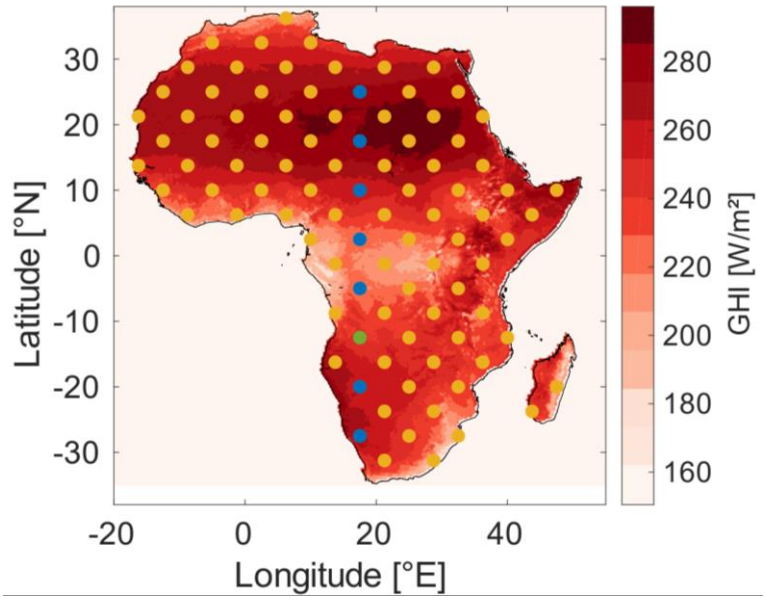


*Figure A.1: Mean annual GHI over the 2008-2015 period from Heliosat SARAH2. The dots are the locations used in the study. The blue ones give a transect and are used in sections 3.3 and 4.1. The green one is used in section 3.1.*

First, a decomposition model [102] is used to compute the direct (DNI) and diffuse (DHI) irradiance from global horizontal irradiance (GHI) and solar angles. Then, the global tilted irradiance (GTI) is calculated using equation A.1.

$$GTI = DNI \cdot cos(\theta) + DHI \quad \text{(A.1)}$$

Where $\theta$ is the "effectiveness" angle, a function of solar angles and panel inclinations and orientation. For this study, we assume that PV panels have a tilt angle equal to the latitude [103] and are oriented towards the south in the northern hemisphere and vice-versa. Then the estimated solar PV production is estimated by equation A.2 as in [104]:

$$P = \eta_{PV} \cdot \left(1 + \alpha(T_m - 25°C)\right) \cdot K_{PV} \cdot \frac{GTI}{1000\, W/m^2} \quad \text{(A.2)}$$

Where $K_{PV}$ $[W_p]$ is the peak power of installed PV panels, $1000\, W/m^2$ corresponds to the irradiance at standard conditions, $\alpha$ is the sensitivity of panel efficiency to the module temperature $T_m$ which is

computed by equation A.3 and $\eta_{PV}$, the panel efficiency that accounts for inverter efficiency and losses of the PV production system.

$$T_m = T_{amb} + \gamma \cdot GTI \quad \text{(A.3)}$$

Where $T_{amb}$ is the ambient temperature (air temperature at 2m from ERA5) and $\gamma$ is a parameter related to the mounting type of the system. A mean value: $\gamma = 0.04°C.m^2/W$ is considered, and the value for crystalline silicon cells: $\alpha = -0.0035/°C$ is taken for the sensitivity of the panel efficiency to temperature [104].

## A.2 Demand data

Figure A.2 shows three different daily load profiles that are estimated from the literature for a fictitious community [105 - 108]. The mean power demand $\overline{D}$ is the same for the three profiles to allow the results to be compared. Productive uses (e.g., mills, pumps, dryers) consume mostly during the day, whereas a domestic load profile is characterized by a high peak demand in the evening and electricity consumption at night. The hybrid load profile stands for a community where both productive and domestic uses can be found.

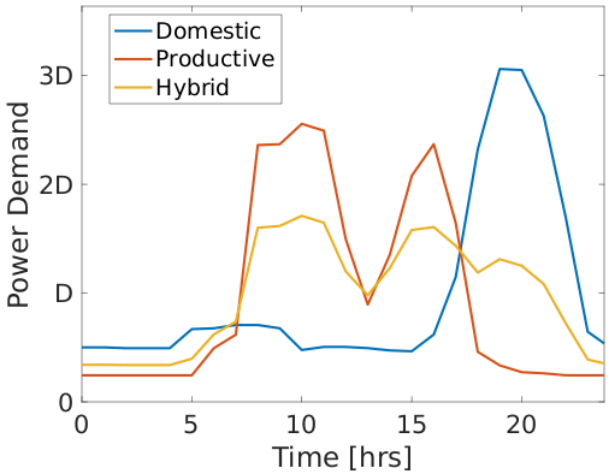


*Figure A.2: Three daily load profiles used in the study.*

In African rural areas, electricity can be used for agricultural activities like irrigation or post-harvest processing [109], which implies that the load profile is different from one season to another. The revenue and expenditure of the population may also vary from one season to the other, impacting the load profile. To account for these seasonal variations, we use sinusoidal yearly load profiles with an amplitude chosen at half of the mean yearly electricity demand (Figure A.3 and equation A.4). Four yearly load profiles are used to account for different periods of high demand, and a yearly profile without seasonality, i.e., the same daily demand throughout the year, is also taken into account.

$$D_d = \overline{D}\left(1 + A\cos\left(2\pi\frac{d - d_{max}}{365}\right)\right) \quad \text{(A.4)}$$

Where $D_d[kW]$ is the daily mean power demand of calendar day $d$, $\overline{D}[kW]$ is the annual mean power demand, $A=0.5$ is the half amplitude of seasonality and $d_{max}$ is the calendar day for the maximum.

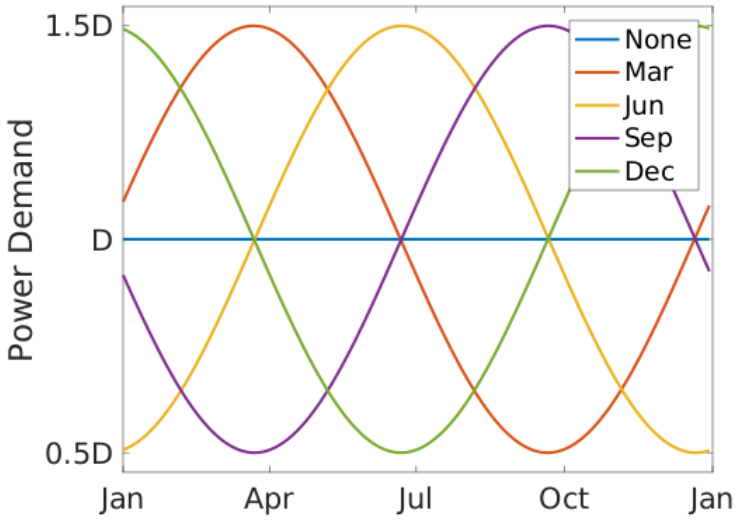


*Figure A.3: The five seasonal patterns considered for the electricity demand. 'Mar,' 'Jun,' 'Sep, 'Dec' account respectively for 'March,' 'June,' 'September' and 'December' and correspond to the months with the highest demand. 'None' is a yearly demand profile without seasonality.*

Thus 15 different load profiles are considered.

As will be shown later, the seasonality of the demand, and more generally the demand/production mismatch (i.e., how these vary from one another), has a significant effect on the results. To characterize this mismatch, we use two indicators as in [74]. The first one, $\sigma_{diff}$, is used to characterize the daily temporal mismatch of the solar resource and the electric demand, and is defined as stated in the equation A.5:

$$\sigma_{diff} = \frac{1}{\overline{D}} \sqrt{\sum_{d}^{N_{days}} \frac{(D_d - P_d^0)^2}{N_{days}}} \qquad \text{A.5}$$

Where $N_{days}$ is the number of days for the simulation period, $D_d$ is the demand per day $d$ and $P_d^0$ is the mean PV production that would be obtained per day $d$ for a system with a PV capacity $K_{PV}^0[kW_p]$. The mean capacity factor (CF) of PV panels, $K_{PV}^0$ is defined as $K_{PV}^0 \cdot CF = \overline{D}$. This corresponds to the capacity that would be required to produce, over the simulation period, an energy amount exactly equal to the total energy of a constant demand $\overline{D}$.

$\sigma_{diff}$ depends on both the seasonal profile of the demand and the variations of the solar resource which derives from top-of-atmosphere (TOA) radiation and atmospheric characteristics (e.g., nebulosity, aerosols).

The second index, nocturnal energy ($NE$), is used to describe the infra-day mismatch between the solar resource and the power demand. It is based on the statistical distribution of the nocturnal energy difference $E_{noct}[kWh]$ estimated each day between the load profile and the PV production profile of said day $P^0(t)$. For any given day, this nocturnal energy difference reflects the energy that must be delivered by the storage or the genset during night-time. The nocturnal energy difference is calculated between midday the day before and midday the day after, by using the equations below.

$$E_{noct}(d) = \sum_{t=-12}^{t=12} P_{noct}^0(t) \cdot 1hr \qquad \text{(A.6)}$$

Where $P_{noct}^0[kW]$ is the nocturnal power difference for each hour $t$ defined as:

$$P^0_{noct}(t) = \begin{cases} D(t) - P^0(t) if D(t) - P^0(t) \geq 0 \\ 0 if D(t) - P^0(t) < 0 \end{cases} \quad \text{(A.7)}$$

The nocturnal energy indicator is then taken as the 75th percentile of the $E_{noct}(d)$ distribution: $NE = p_{75}(E_{noct}(d))$. For more details on these two indicators of the temporal mismatch between solar resource and electric demand, please refer to [76].

The fuel consumption $f_{conso}(t)[L]$at time *t* is estimated as:

$$f_{conso}(t) = \frac{E_{gen}(t)}{HV_f * \eta_{gen}\left(\frac{P_{gen}(t)}{K_{gen}}\right)} \quad \text{(A.8)}$$

Where $E_{gen}(t)[kWh]$ is the electrical energy to be supplied by the genset at time *t*, where $P_{gen}(t)[kW]$ and $\eta_{gen}$ [-] are the genset power and efficiency, and $K_{gen}$ its nominal power, and where $HV_f = 10\,kWh/L$ is the heating value of diesel. Following [110,111], the genset efficiency is considered as a function of its load factor $\frac{P_{gen}(t)}{K_{gen}}$ (Figure A.4).

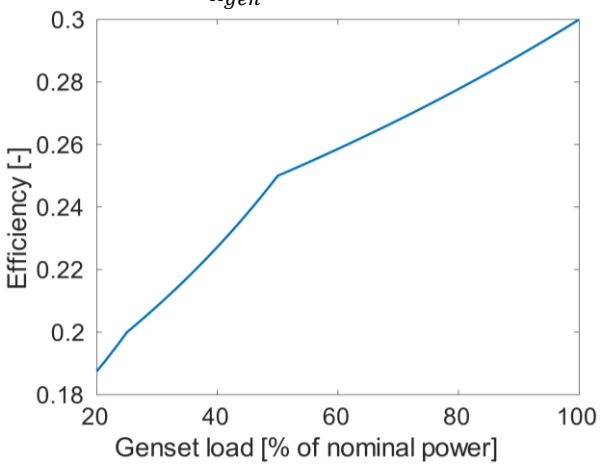


*Figure A.4: Genset efficiency $\eta_{gen}$as a function of its load factor $P_{gen}/K_{gen}$. This efficiency is the ratio of the electricity output of the genset on the thermal energy from the fuel.*

## A.3 CFP calculation

The CFP is calculated per kWh of supplied energy. This encompasses the emissions related to the whole life cycle of the components, from the mining of the material needed and the manufacturing to the end-of-life of the components. The total $CFP_{tot}[t_{CO_2}]$ of the MG is estimated from the CFP values of the different MG components:

$$CFP_{tot} = K_{bat}CFP_{bat}\frac{L}{L_{bat}} + K_{PV}CFP_{PV} + K_{gen}CFP_{gen}\frac{L}{L_{gen}} + CFP_{fuel}F_{conso} \quad \text{(A.9)}$$

Where $K_{bat}[kWh]$, $K_{PV}[kW_p]$, $K_{gen}[kW]$ are respectively the capacity installed for the batteries, the PV panels and the genset; $CFP_{bat}[t_{CO_2}/kWh]$, $CFP_{gen}[t_{CO_2}/kW]$, $CFP_{fuel}[t_{CO_2}/L]$ and $CFP_{PV}[t_{CO_2}/kW_p]$ are respectively the CFP associated to $1kWh$ of installed batteries, $1kW_p$ of installed PV, $1kW$ of genset power capacity and $1L$ of fuel; $F_{conso}[L]$ is the fuel consumption over the lifetime of the project $L[yrs]$ ; $L_{bat}[yrs]$ and $L_{gen}[yrs]$ are respectively the lifetime of batteries and genset. We consider a project lifetime of 15 years, so that the PV panel does not need to be replaced. The genset lifetime in years $L_{gen}$ is derived from a lifetime expressed in functioning hours

$L_{gen,hrs}[hrs]$ using equation A.10 with $F_{use}[hrs]$ as the number of the genset use hours over the whole project lifetime:

$$L_{gen} = \frac{L_{gen,hrs}}{F_{use}/L} \quad \text{(A.10)}$$

Finally, the CFP per $kWh$ of energy supplied $CFP$ is given by equation A.11:

$$CFP = \frac{CFP_{tot}}{E_{supply}} \quad \text{(A.11)}$$

Where $E_{supply}[kWh]$ is the energy supplied over the project lifetime. As the demand must be met at all times, $E_{supply}$ corresponds to the total energy demand over the project lifetime.
Values taken for the different parameters used in this calculation are given in Table A.1 and correspond to the mean values estimated by Besseau [27] who compiled the results of multiple life-cycle analysis mostly from the EcoInvent Database.

*Table A.1: Parameter values used for the CFP calculation. $CFP_{PV}$ and $CFP_{Bat}$ also include the CFP for inverters.*

| $CFP_{bat}[t_{CO_2}/kWh]$ | $CFP_{PV}[t_{CO_2}/kW_p]$ | $CFP_{gen}[t_{CO_2}/kW]$ | $CFP_{fuel}[t_{CO_2}/L]$ |
|---|---|---|---|
| 0.3 | 1 | 0.02 | $2.6\text{x}10^{-3}$ |

| $L[yrs]$ | $L_{bat}[yrs]$ | $L_{gen,hrs}[hrs]$ |
|---|---|---|
| 15 | 7 | 25000 |

## A.4 LCOE calculation

The cost related to the distribution system is not included in the $LCOE$ calculation. As for the CFP, total system costs are estimated using costs by unit of installed component and by litre of diesel fuel consumption (equation A.12).

$$C_{tot} = K_{bat}\alpha_{bat} + K_{PV}\alpha_{PV} + K_{gen}\alpha_{gen} + C_{fuel}\sum_{yr=1}^{L}\frac{F_{conso,yr}}{(1+d)^{yr}} \quad \text{(A.12)}$$

Where $C_{fuel}[\$/L]$ is the cost of $1L$ of fuel, $F_{conso,yr}[L]$ is the fuel consumption for one year; $d$ is the discount rate and $\alpha_{bat}$ [-], $\alpha_{PV}$ [-] and $\alpha_{gen}$ [-] are the costs related to installation, replacement and maintenance of the components over their lifetime, as shown by equations A.13, A.14 and A.15.

$$\alpha_{bat} = C_{bat}.\left(\frac{1-(1+d)^{(L+L_{bat})}}{(1+d)^{L}-(1+d)^{(L+L_{bat})}} + \sum_{k=1}^{L}\frac{P_{OM,bat}}{(1+d)^{k}}\right) \quad \text{(A.13)}$$

$$\alpha_{PV} = C_{PV}.\left(1 + \sum_{k=1}^{L}\frac{P_{OM,PV}}{(1+d)^{k}}\right) \quad \text{(A.14)}$$

$$\alpha_{gen} = C_{gen}.\left(\frac{1-(1+d)^{(L+L_{gen})}}{(1+d)^{L}-(1+d)^{(L+L_{gen})}} + \sum_{k=1}^{L}\frac{P_{OM,gen}}{(1+d)^{k}}\right) \quad \text{(A.15)}$$

Where $C_{bat}[\$/kWh]$, $C_{PV}[\$/kW_p]$, $C_{gen}[\$/kW]$ are respectively the installation costs associated to $1kWh$ of installed batteries, $1kW_p$ of installed PV and $1kW$ of genset; and $P_{OM,bat}$ [-], $P_{OM,PV}$ [-] and $P_{OM,gen}$ [-] are proportionality coefficients between investment and maintenance costs related to each component. Maintenance and operation costs are assumed to be time invariant and proportional to

the investment cost of each component. The mean values considered for the different parameters are given in Table A.2 [112-114].

*Table A.2: Parameter values for the LCOE calculation, lifetimes of components are given in Table A.1, $C_{PV}$ and $C_{Bat}$ also include the costs of inverters.*

| $C_{bat}[\$/kWh]$ | $C_{PV}[\$/kW_p]$ | $C_{gen}[\$/kW]$ | $C_{fuel}[\$/L]$ |
|---|---|---|---|
| 350 | 1900 | 500 | 1 |

| $P_{OM,bat}$ [%] | $P_{OM,PV}$ [%] | $P_{OM,gen}$ [%] | $d$ [%] |
|---|---|---|---|
| 3 | 2 | 10 | 10 |

Finally, the LCOE is computed with equation A.16:

$$LCOE = \frac{C_{tot}}{\sum_{k=1}^{L} \frac{E_{supply}}{(1+d)^k}} \quad \text{(A.16)}$$

## A.5 Sensitivity Analysis

Scenarios considered for the analysis:

The goal of this sensitivity analysis is to see how variable are the results found in section 3 when modifying the discount rate $d$, the costs ($C_{bat}$, $C_{PV}$, $C_{fuel}$), the CFP ($CFP_{bat}$, $CFP_{PV}$, $CFP_{fuel}$) and the lifetimes ($L_{bat}$,$L$, $L_{gen,hrs}$) related to each component. For each of these parameters, 3 values are taken: the reference value (Table A.1 and Table A.2) and variations of ±50% from this reference value (with two exceptions for $CFP_{fuel}$ : ±10% and $L$ : ±33%). These variations are representative of the variability for these parameters as described in [27,112-114]. The analysis is performed on the 8 locations of the NS transect presented in Figure A.1 and for the 15 load profiles presented in section A.2 (Domestic, Productive, Hybrid with or without seasonality). Thus, it allows us to estimate the sensitivity of the results related to the mean capacity factor and the mismatch indicators between the solar resource and the demand. Combining all these variations give us around 7 million different scenarios for which we compute lowest LCOE and lowest CFP configurations.

To summarize the results of this sensitivity analysis and to better see the impact of each parameter, it is possible to look at the relative difference of CFP and LCOE results when modifying only one parameter. The calculation of the sensitivity for each parameter is made for the 8 N-S transect locations, for each demand profile and for each scenario of cost and CFP related to component. Table A.3 gives an example of how to calculate the sensitivity for some scenarios, a location in Angola and a hybrid demand profile without seasonality.

| Scenario for other parameters $[d; L_{bat}; L; L_{gen,hrs}; CFP_{bat}; CFP_{PV}; CFP_{fuel}; C_{fuel}; C_{bat}]$ | Sensitivity to $C_{PV}$ | | | |
|---|---|---|---|---|
| | -50% | 0% | 50% | *Sensitivity value* |
| [0%, 0%, 0%, 0%, -50%, -50%, -10%, -50%, -50%] | **-17%** | **+6%** | **+6%** | 0.23 |
| [0%, 0%, 0%, 0%, -50%, -50%, -10%, -50%, -25%] | **-12%** | **+4%** | **+4%** | 0.16 |
| [0%, 0%, 0%, 0%, -50%, -50%, -10%, -50%, 0%] | **-10%** | **+3%** | **+3%** | 0.12 |
| … | **…** | **…** | **…** | |

| | | | | |
|---|---|---|---|---|
| [0%, 0%, 0%, 0%, +50%, +50%, +10%, +50%, +50%] | **-18%** | **+1%** | **+16%** | 0.34 |

*Table A.3 : Calculation of the sensitivity of the lowest LCOE when changing $C_{PV}$ for different scenario. Values in bold corresponds to the relative change of the lowest LCOE value compared to the mean of these 3 LCOE values. The sensitivity is then the slope of the linear regression between these relative changes and the $C_{PV}$ variations.*

This sensitivity calculation is done for the performance (LCOE and CFP) of the lowest CFP and lowest LCOE configurations leading to 4 distributions of sensitivities for each parameter. These distributions are reported in Figure 11.

# Appendix B. Supplementary figures

## B.1 Supplementary figures for section 3.1: Carbon footprint vs. direct GHG emissions of a mini-grid

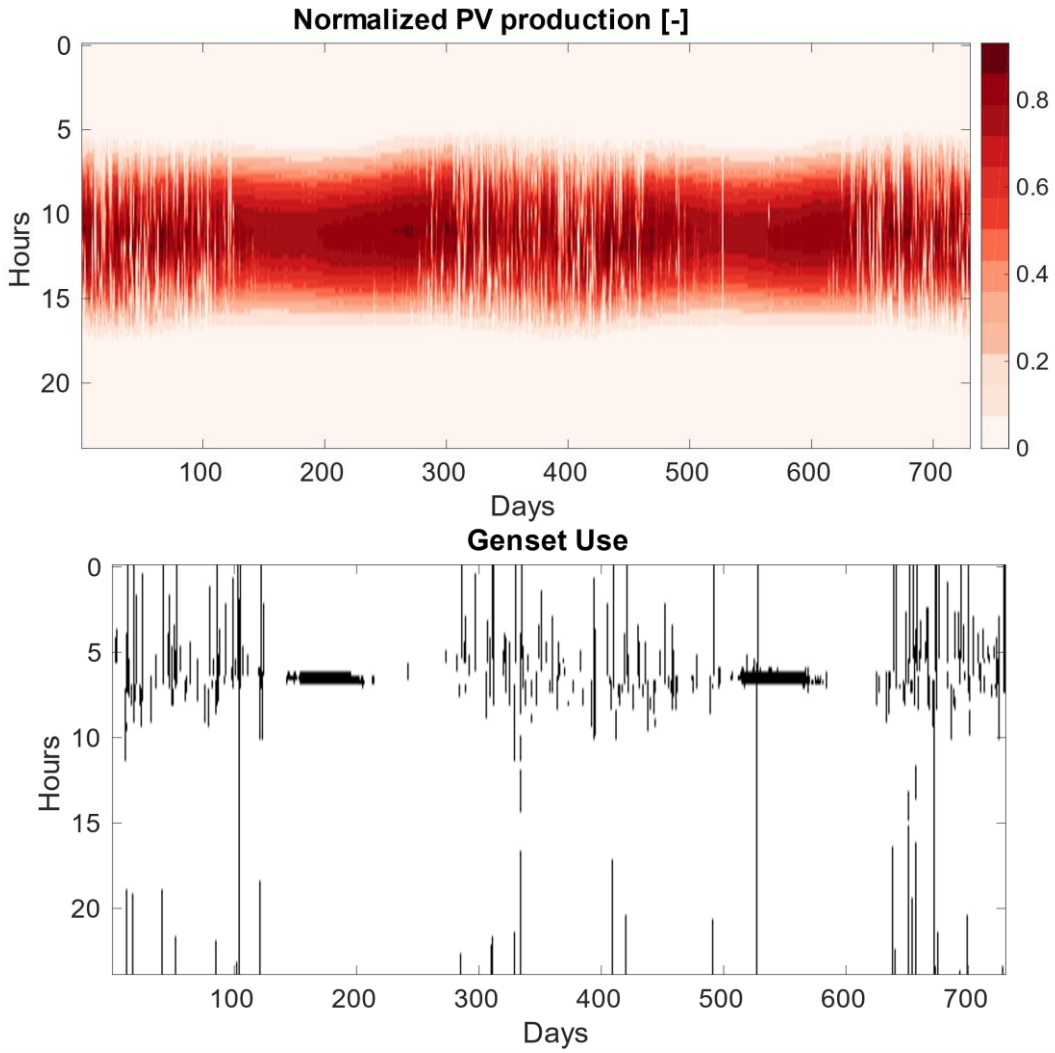


*Figure B.1: Distribution of the solar capacity factor (top) and of the genset use timestep (bottom) over the two years used in the simulation. The genset is mainly used when the daily solar resource is low (days 0 to 120, 300 to 450 and 250 to 730) and at the end of the night (around 6 am).*

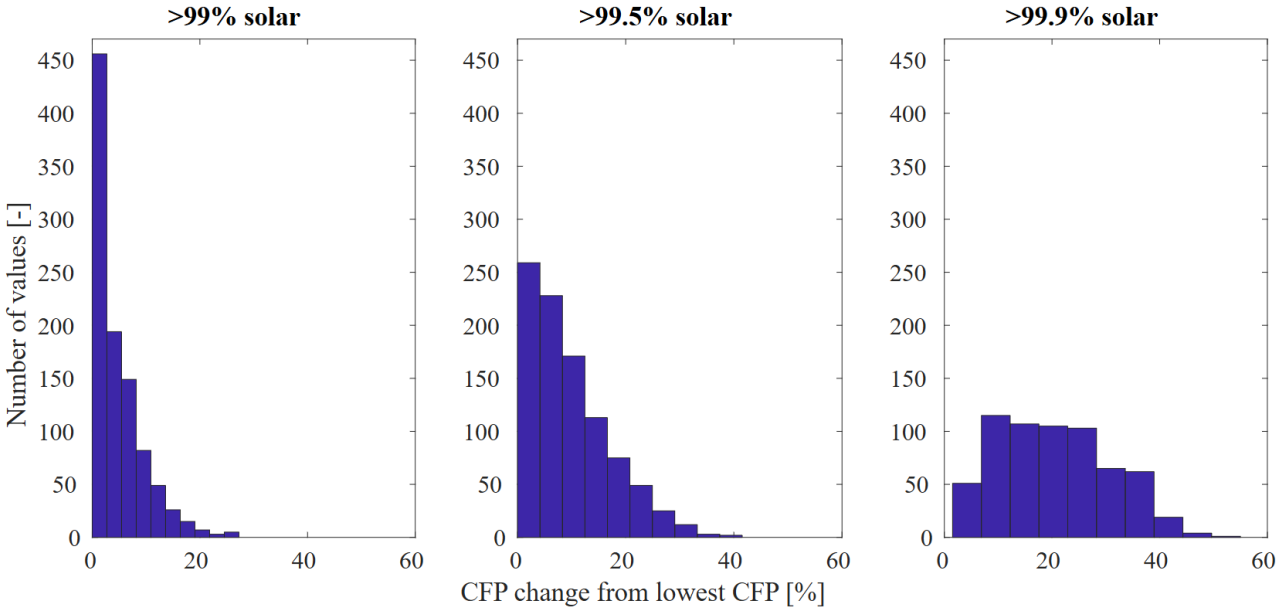


*Figure B.2: Distributions of the relative difference between CFP* and the configurations with lowest CFP that satisfy a constraint of diesel supply (<1%, <0.5% or <0.1%). The total number of values per histogram is 1395 and corresponds to the simulation for 93 locations and 15 different load profiles. Imposing a strong constraint (>99%) on the proportion of energy covered by solar PV increases the CFP of MG compared to the CFP* value.*

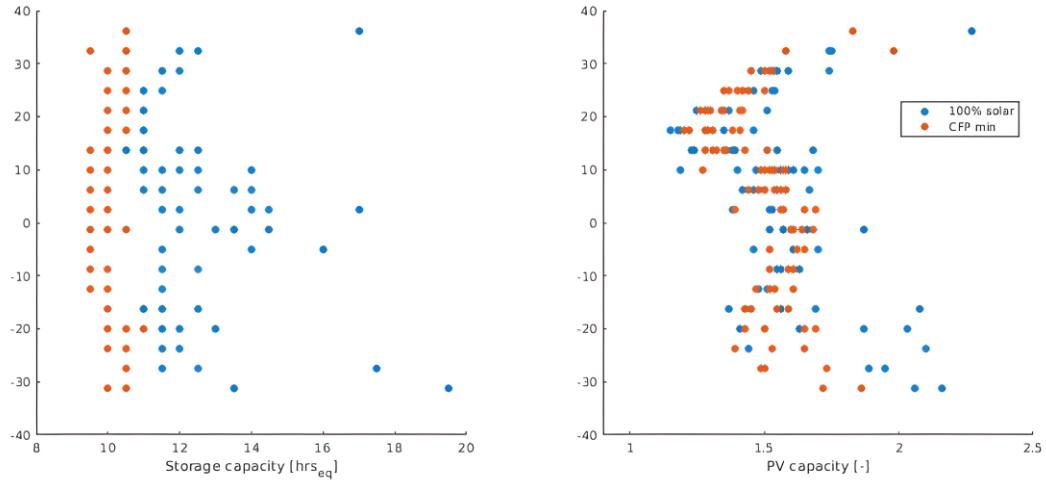


*Figure B.3 : Configurations (PV and storage capacities) for the CFP* configurations (red) and configurations which supply more than 99% of the energy with solar PV (blue). This figure shows only the result for a hybrid load profile without seasonality. Imposing a strong constraint (>99%) on the proportion of energy covered by solar PV increases the storage capacity, whereas the PV capacity stays similar.*

## B.2 Supplementary figures for section 3.2: The influence of solar resource on LCOE* and CFP* values

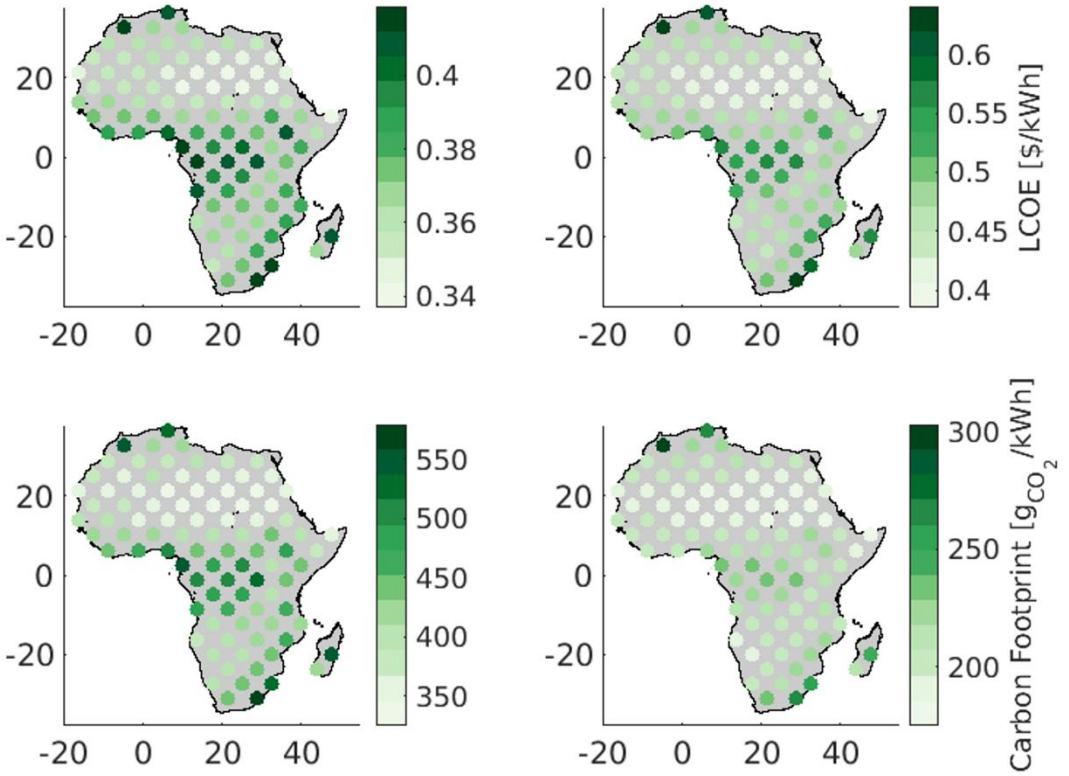


*Figure B.4: LCOE and CFP of the lowest LCOE (left column) and lowest CFP (right column) configurations obtained for a hybrid load profile without seasonality. LCOE and CFP for a diesel only configuration are respectively equal to 0.46$/kWh and 996gCO2/kWh. The CFP of the LCOE* configuration is around twice the CFP of the CFP* configurations. The CFP* configurations increase the LCOE by 25 to 50% compared to the LCOE* configurations.*

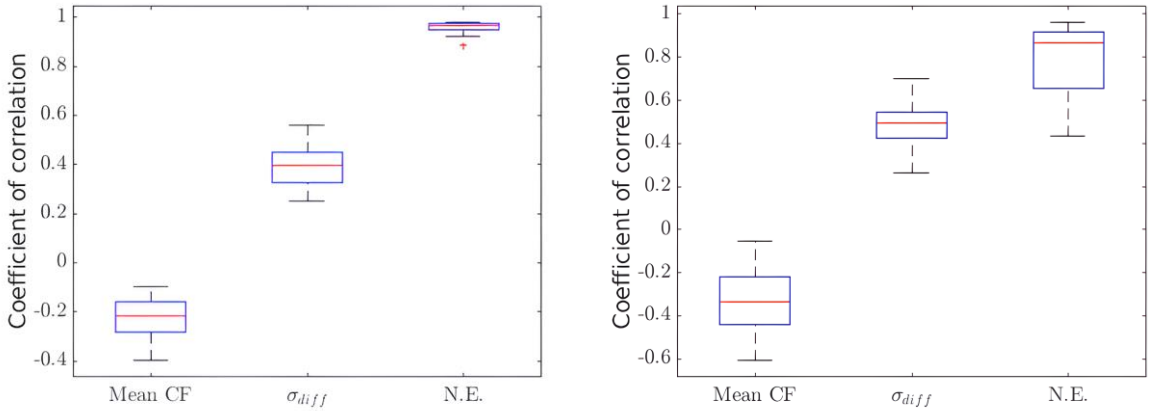


*Figure B.5: Distribution of the coefficient of correlation between the solar and demand characteristics (CF, $\sigma_{diff}$ and NE) and the CFP* values (left) or the LCOE* values (right). Each coefficient is computed on the 93 locations and 15 load profiles, and one scenario of CFP, costs and lifetimes per components. All the coefficients have a p-value below 0.001. Boxplots show the distribution for 27 scenarios of costs (LCOE*) or 27 scenarios of environmental parameters (CFP*). The LCOE* and CFP* values are strongly correlated to the mismatch between the solar production and electric demand even if the economic and environmental assumptions are different.*

## B.3 Supplementary figures for section 3.4: The possibility for trade-off configurations between LCOE* and CFP*

Figures B.6 and B.7 show that the shape of the envelope curve can strongly vary when modifying the socio-economic, environmental and technical assumptions. The common shape presented in section 3.4 (Figure 9) and also presented in different articles [56, 73, 75] is not always valid.

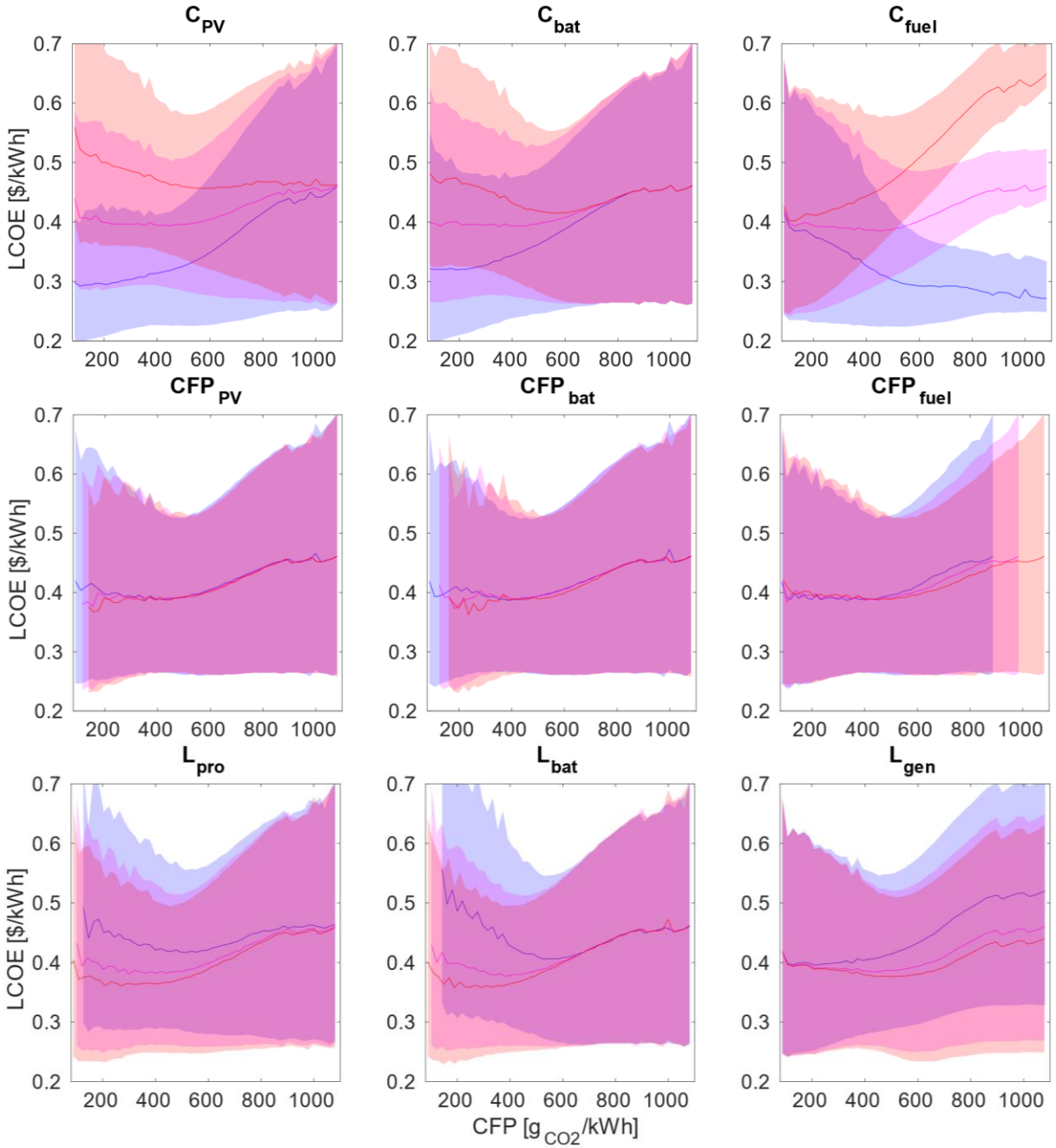


*Figure B.6: Envelope curves for different scenarios of costs, CFPs and lifetimes of a location in Angola (-12.5°N,17.5°E) and for a hybrid load profile without seasonality. The $C_{PV}$ graph represents the variation of the Envelope curves when changing the value of $C_{PV}$, the red colour corresponds to an increase of 50% of the $C_{PV}$ value whereas the blue one corresponds to a decrease of 50% and the purple one is obtained with the reference value of $C_{PV}$. The area represents the variations of this curve when modifying the other parameters as specified in Appendix B. The upper limit of the area is the 90$^{th}$ percentile of values and the lower limit is the 10$^{th}$ percentile. The same applies to the other graphs, apart for $CFP_{fuel}$ where variations are only of ±10% and for L with variations of ±33%.*

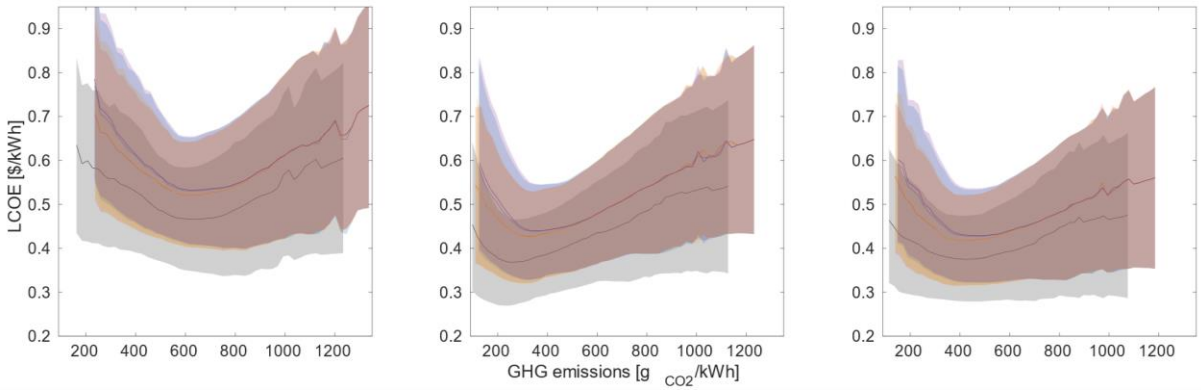


*Figure B.7 : Envelope curves for different load profile of a location in Angola (-12.5°N,17.5°E). Each graph corresponds to a daily load profile: Domestic, Productive and Hybrid and colours account for the seasonality: blue, red, yellow and purple corresponds respectively to a peak consumption in March, June, September and December. The black one is obtained for load profiles without seasonality. The area represents the variations of this curve when modifying all the costs and CFP as specified in section Appendix B. The upper limit of the area is the 90$^{th}$ percentile of values and the lower limit is the 10$^{th}$ percentile.*

Considering a hybrid load profile with the mean values for economic, technical and environmental assumptions as in section 3.4, we found that a small or moderate increase in LCOE relative to LCOE* can achieve a significant reduction in CFP (Figure 10).

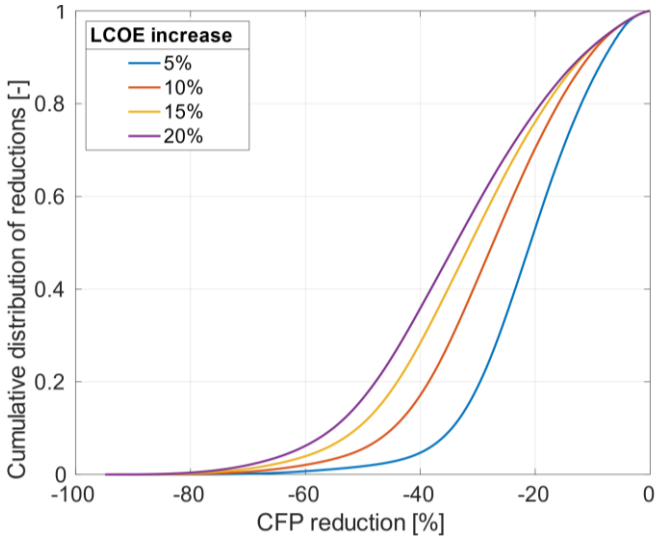


*Figure B.8: Cumulative distribution of the CFP relative change from the LCOE* configurations related to all the scenarios (8 locations x 15 demand profiles x 59 049 sets of technical, economic and environmental assumptions) of the sensitivity analysis. The different curves correspond to different levels of LCOE increase from the LCOE* configuration. This figure is built as follow: for each combination of location, demand profile and scenario, the LCOE* configuration is identified. Then, the configurations with a higher CFP or a LCOE higher than X% (5, 10, 15 or 20) are excluded. Among these configurations, the one with the lowest CFP is identified and the CFP reduction from the LCOE* configuration is calculated. Each distribution contains all these CFP reductions calculated for each combination of location, demand profile and set of assumptions.*

In the following, we use the term "scenario" to refer to a combination of a location, a load profile and a set of economic, technical and environmental assumptions.

This result, however, does not necessarily hold true for all possible costs, CFP, lifetimes, and load profile scenarios. Among the different scenarios considered for the sensitivity analysis, a 10% LCOE increase leads to a CFP reduction of over 40% in only 20% of cases. This result may seem disappointing at first. Note, however, that the CFP distance between LCOE* and CFP* configurations depends greatly on the scenario and that, for certain scenarios, this distance limits the possibility of emission reductions. A 10% increase in LCOE would, for instance, lead to a CFP reduction of less

than 20% in around 30% of cases. However, this 30% of cases decreases to 12% if we remove the configurations in which the CFP distance between the CFP* and the LCOE* is below 20% (Appendix A, Table A.1). Thus, even if this mean CFP reduction (20%) is considerably lower than that presented in the Results section (40%), it is still significant for most of the scenarios considered here.

Note that the configurations that only allow for a small CFP reduction correspond to low fuel costs (Appendix A, Table A.2). For a domestic profile, low CFP reduction potential corresponds to short-lifetime, high-cost batteries. For productive and hybrid load profiles, it corresponds to high PV costs and a high discount rate. However, scenarios with a low fuel cost, a high cost for PV and a high discount rate do not automatically lead to a low CFP reduction. In the results of our analysis, only 50% of these scenarios lead to a CFP reduction below 20% for a 10% LCOE increase (Table A.2). More details can be found in Appendix A, Tables A.2 and A.3.

| | | CFP reduction from the LCOE* configuration [%] | | | | | |
|---|---|---|---|---|---|---|---|
| | | 10 | 20 | 30 | 40 | 50 | 60 |
| Accepted LCOE increase [%] | 5 | 7.8 | 36 | 71 | 90 | 95 | 97 |
| | 10 | 1.4 | 12 | 35 | 65 | 84 | 90 |
| | 15 | 0.20 | 4.9 | 18 | 42 | 68 | 81 |
| | 20 | 0.041 | 2.1 | 9.9 | 27 | 52 | 71 |

*Table B.1 : CFP reduction from the LCOE* configuration when allowing an increase of LCOE. These numbers refer to the sensitivity analysis (Figure B.10) and are given in %. Scenarios where the CFP relative change between LCOE* and CFP* is lower than the CFP reduction wanted are excluded. For instance, the 12% (red value in the table) means that, when excluding all the scenarios where the CFP* and LCOE* configurations have a CFP relative difference below 20%, a 10% LCOE increase gives a CFP reduction lower than 20% in 12% of the scenarios.*

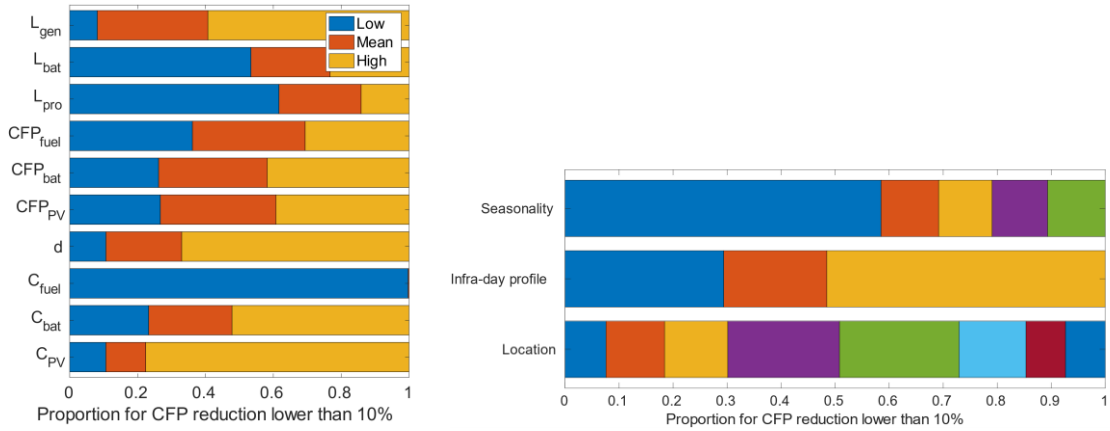


*Figure B.9 : Proportion of scenarios (all combination of location, demand profile and set of technical, economic and environmental assumptions) with the different parameters values for a 10% LCOE increase and a CFP reduction lower than 10%. Scenarios where the CFP relative change between LCOE* and CFP* is lower than 10% are excluded. Left and right legends are different. On the left graph, the 'low', 'medium' and 'high' values corresponds to the value given in Appendix A.5. 'Low' corresponds to a decrease of the mean value by 50% (33% for $L_{pro}$ and 10% for $CFP_{fuel}$). 'High' corresponds to a decrease by 50% (33% for L and 10% for $CFP_{fuel}$) of the mean value. On the right graph, the colours refer to the load profile characteristics and location of the N-S transect (Figure A.1). For the Seasonality, from left to right, colours correspond to 'No seasonality', 'March', 'June', 'September', 'December' (month of the highest demand). For the Infra-day load profile, they correspond to 'Domestic', 'Productive', 'Hybrid'. For the Location, they correspond to the 8 locations of the transect (17.5°E) from -27.5°N to 25°N with a step of 7.5°N.*

| Combination of parameters | | | | | | | CFP reduction [%] | | |
|---|---|---|---|---|---|---|---|---|---|
| $C_{fuel}$ | $C_{PV}$ | $d$ | $C_{bat}$ | $L_{bat}$ | Infra-day | Seasonality | 10 | 15 | 20 |
| Low | | | | | | | 2.9 | 9.6 | 17.7 |
| Low | High | | | Low | | | **8.0** | 26 | 42 |

| | | | | | | | | | |
|---|---|---|---|---|---|---|---|---|---|
| Low | High | High | High | Low | | | 18 | 50 | 69 |
| Low | | | | | Hybr/Prod | None | 9.6 | 20 | 26 |
| | High | | | | Hybr/Prod | None | 9.4 | 18 | 23 |
| Low | High | High | | | | | 14 | 37 | 53 |
| | High | High | | | Hybr/Prod | | 7.1 | 17 | 24 |
| Low | High | High | | | Hybr/Prod | None | 63 | 93 | 95 |
| Low | | | | | Dom | None | 5.9 | 16 | 30 |
| | | | | Low | Dom | None | 7.9 | 22 | 36 |
| Low | | | High | Low | | | 9.5 | 30 | 45 |
| | | | High | Low | Dom | | 7.6 | 28 | 46 |
| Low | | | High | Low | Dom | None | 44 | 76 | 88 |

*Table B.2 : Proportion of scenarios that give a CFP reduction lower than 10, 15 and 20% for a LCOE increase of 10% for different combination of parameters value. For instance, the 8.0% (red value in the table) means that, on all the scenarios with a low value of $C_{fuel}$ and $L_{bat}$, and a high value of $C_{PV}$, 8% of scenarios give a CFP reduction lower than 10%. 'Low' corresponds to a decrease of the mean value by 50% (33% for $L_{pro}$ and 10% for $CFP_{fuel}$). 'High' corresponds to a decrease by 50% (33% for $L_{pro}$ and 10% for $CFP_{fuel}$) of the mean value.*

| Combination of parameters | | | | | | | CFP reduction [%] | | |
|---|---|---|---|---|---|---|---|---|---|
| $C_{fuel}$ | $C_{PV}$ | $d$ | $C_{bat}$ | $L_{bat}$ | Infra-day | Seasonality | 20 | 30 | 40 |
| Low | | | | | | | 3.7 | 13 | 26 |
| Low | High | | | Low | | | 10 | 30 | 43 |
| Low | High | High | High | Low | | | 19 | 57 | 74 |
| Low | | | | | Hybr/Prod | None | 5.5 | 15 | 25 |
| | High | | | | Hybr/Prod | None | 5.1 | 14 | 19 |
| Low | High | High | | | | | 9.2 | 33 | 56 |
| | High | High | | | Hybr/Prod | | 3.8 | 13.5 | 23 |
| Low | High | High | | | Hybr/Prod | None | 36 | 71 | 82 |
| Low | | | | | Dom | None | 11.5 | 29 | 54 |
| | | | | Low | Dom | None | 15 | 31 | 35 |
| Low | | | High | Low | | | 19 | 39 | 45 |
| | | | High | Low | Dom | | 20 | 39 | 41 |
| Low | | | High | Low | Dom | None | 67 | 82 | 69 |

*Table B.3 : Same table as Table B.2 with a 20% LCOE increase.*

## B.4 Supplementary figures for section 4.2: Estimating the cost of a CFP reduction policy

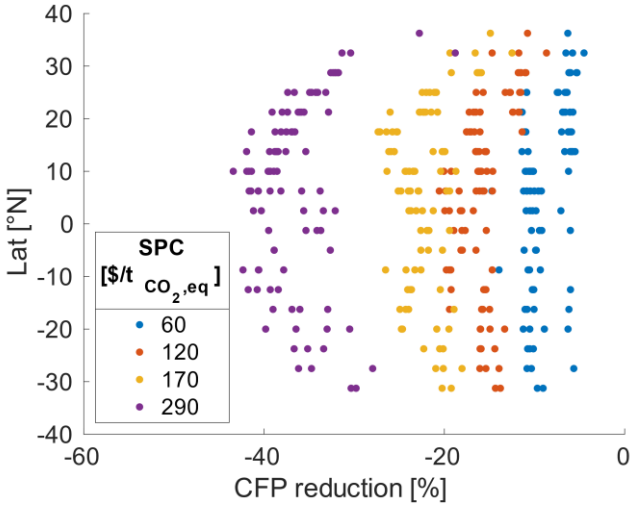


*Figure B.10 : CFP reduction from the LCOE* configuration as a function of the latitude when adding different values of shadow carbon prices (SPC) taken from the IPCC report [4]. To limit warming to 2°C, the SPC for 2030 estimated by the IPCC (2022) would need to be between 60$/tCO2 and 120$/tCO2. To limit warming to 1.5°C, it would have to be around 170-290$/tCO2. The lowest value of 60$/tCO2 already allows a 5 to 10% reduction of the CFP compared to the LCOE* configuration. The low SPC value to limit global warming to 1.5°C (170$/tCO2) allows a more than 20% reduction of the CFP.*

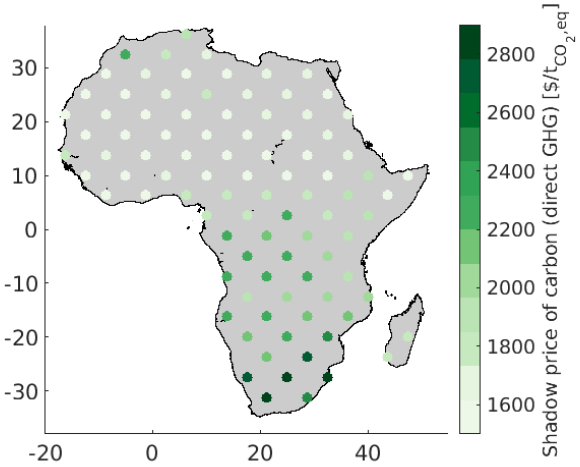


*Figure B.11: Shadow price of carbon to go from the LCOE* to CFP* configurations (same diesel consumption) considering only direct GHG emissions.*

## References:


[1] International Energy Agency, « Africa Energy Outlook 2022 », 2022.

[2] United Nations, « UN Sustainable Development Goals ». [En ligne]. Disponible sur: https://sdgs.un.org/goals/goal7

[3] « Nationally Determined Contributions (NDCs) ». Consulté le: 21 janvier 2022. [En ligne]. Disponible sur: https://unfccc.int/process-and-meetings/the-paris-agreement/nationally-determined-contributions-ndcs/nationally-determined-contributions-ndcs

[4] IPCC, « Climate Change 2022: Mitigation of Climate Change. Contribution of Working Group III to the Sixth Assessment Report of the Intergovernmental Panel on Climate Change », Cambridge University Press, Cambridge, UK and New York, NY, USA, 2022. doi: 10.1017/9781009157926.

[5] Olubusoye, Olusanya Elisa, Dasauki Musa, and Salvatore Ercolano. 2020. “CARBON EMISSIONS AND ECONOMIC GROWTH IN AFRICA: ARE THEY RELATED?” Cogent Economics & Finance 8 (1). doi:10.1080/23322039.2020.1850400.
[6] Mpofu FY. Green Taxes in Africa: Opportunities and Challenges for Environmental Protection, Sustainability, and the Attainment of Sustainable Development Goals. Sustainability. 2022; 14(16):10239. https://doi.org/10.3390/su141610239
[7] Olumuyiwa T. Amusan, Nnamdi I. Nwulu, Saheed L. Gbadamosi, Techno-economic analysis of hybrid solar-biomass-wind for water pumping considering carbon tax and renewable energy rebate, Energy Reports, Volume 10, 2023, Pages 3941-3954, ISSN 2352-4847, https://doi.org/10.1016/j.egyr.2023.10.054.
[8] Yiadom, Eric B., Lord Mensah, Godfred A. Bokpin, and John K. M. Mawutor. 2024. “Carbon Tax Adoption and Foreign Direct Investment: Evidence from Africa.” Cogent Economics & Finance 12 (1). doi:10.1080/23322039.2024.2312783.
[9] Timilsina, Govinda R., Yazid Dissou, Michael Toman, and Dirk Heine. 2023. “How Can a Carbon Tax Benefit Developing Economies with Informality? A CGE Analysis for Côte d’Ivoire.” Climate Policy 24 (1): 71–86. doi:10.1080/14693062.2023.2223530.
[10] M. Moustapha Maman Ali, Qian Yu, Assessment of the impact of renewable energy policy on sustainable energy for all in West Africa, Renewable Energy, Volume 180, 2021, Pages 544-551, ISSN 0960-1481, https://doi.org/10.1016/j.renene.2021.08.084.
[11] M. Moner-Girona, R. Ghanadan, M. Solano-Peralta, I. Kougias, K. Bódis, T. Huld, S. Szabó, Adaptation of Feed-in Tariff for remote mini-grids: Tanzania as an illustrative case, Renewable and Sustainable Energy Reviews, Volume 53, 2016, Pages 306-318, ISSN 1364-0321, https://doi.org/10.1016/j.rser.2015.08.055.
[12] Green Climate Fund, « GCF at a glance », Green Climate Fund. Consulté le: 7 décembre 2022. [En ligne]. Disponible sur: https://www.greenclimate.fund/document/gcf-glance
[13] « Green Mini-Grids », SEforALL Africa Hub. Consulté le: 9 novembre 2022. [En ligne]. Disponible sur: https://www.se4all-africa.org/seforall-in-africa/regional-initiatives/green-mini-grids/
[14] Tariq G, Sun H, Ali S. Environmental footprint impacts of green energies, green energy finance and green governance in G7 countries. Carbon Footprints. 2024; 3(1): 5. http://dx.doi.org/10.20517/cf.2023.48
[15] Paul Adjei Kwakwa, Sectoral growth and carbon dioxide emission in Africa: can renewable energy mitigate the effect?, Research in Globalization, Volume 6, 2023, 100130, ISSN 2590-051X, https://doi.org/10.1016/j.resglo.2023.100130.
[16] Nyantakyi, G., Gyimah, J., Sarpong, F.A. et al. Powering sustainable growth in West Africa: exploring the role of environmental tax, economic development, and financial development in shaping renewable energy consumption patterns. Environ Sci Pollut Res 30, 109214–109232 (2023). https://doi-org.sid2nomade-1.grenet.fr/10.1007/s11356-023-30034-5
[17] FengSheng Chien, Trong Lam Vu, Thi Thu Hien Phan, Sang Van Nguyen, Nguyen Ho Viet Anh, Thanh Quang Ngo, Zero-carbon energy transition in ASEAN countries: The role of carbon finance, carbon taxes, and sustainable energy technologies, Renewable Energy, Volume 212, 2023, Pages 561-569, ISSN 0960-1481, https://doi.org/10.1016/j.renene.2023.04.116.
[18] Wagner Wilson Bortoletto, Antonio Carlos Pacagnella Junior, Otavio Gomes Cabello, Exploring the scientific literature on clean development mechanisms: A bibliometric analysis, Energy Policy,Volume 183, 2023, 113806, ISSN 0301-4215, https://doi.org/10.1016/j.enpol.2023.113806.
[19] Igor Makarov, Sedat Alataş, Production- and consumption-based emissions in carbon exporters and importers: A large panel data analysis for the EKC hypothesis, Applied Energy, Volume 363, 2024, 123063, ISSN 0306-2619,https://doi.org/10.1016/j.apenergy.2024.123063.
[20] Beaufils, T., Ward, H., Jakob, M. et al. Assessing different European Carbon Border Adjustment Mechanism implementations and their impact on trade partners. Commun Earth Environ 4, 131 (2023). https://doi.org/10.1038/s43247-023-00788-4

[21] Michael Jakob, “Why carbon leakage matters and what can be done against it”, One Earth,| Volume 4, ISSUE 5, P609-614, May 21, 2021, DOI: https://doi.org/10.1016/j.oneear.2021.04.010
[22] Kris R Voorspools, Els A Brouwers, William D D'haeseleer, Energy content and indirect greenhouse gas emissions embedded in ‘emission-free’ power plants: results for the Low Countries, Applied Energy, Volume 67, Issue 3, 2000, Pages 307-330, ISSN 0306-2619, https://doi.org/10.1016/S0306-2619(00)00016-7.
[23] Feng Liu, Jeroen C.J.M. van den Bergh, Differences in CO2 emissions of solar PV production among technologies and regions: Application to China, EU and USA, Energy Policy, Volume 138, 2020, 111234, ISSN 0301-4215, https://doi.org/10.1016/j.enpol.2019.111234.
[24] R. Frischknecht, P. Stolz, L. Krebs, M. De Wild-Scholten, et P. Sinha, « Life Cycle Inventories and Life Cycle Assessments of Photovoltaic Systems », Report IEA-PVPS T12-19:2020, déc. 2020.
[25] T. Le Varlet, O. Schmidt, A. Gambhir, S. Few, et I. Staffell, « Comparative life cycle assessment of lithium-ion battery chemistries for residential storage », J. Energy Storage, vol. 28, p. 101230, avr. 2020, doi: 10.1016/j.est.2020.101230.
[26] M. Grágeda, M. Escudero, W. Alavia, S. Ushak, V. Fthenakis, « Review and multi-criteria assessment of solar energy projects in Chile », Renew. Sustain. Energy Rev., vol. 59, p. 583596, juin 2016, doi: 10.1016/j.rser.2015.12.149.
[27] Romain Besseau, 2019, « Analyse de cycle de vie de scénarios énergétiques intégrant la contrainte d’adéquation temporelle production-consommation », Thèse de doctorat Energétique et génie des procédés Paris Sciences et Lettres (ComUE) 2019, http://www.theses.fr/2019PSLEM068/document
[28] Yu Gan, Amgad Elgowainy, Zifeng Lu, Jarod C Kelly, Michael Wang, Richard D Boardman and Jason Marcinkoski, “Greenhouse gas emissions embodied in the U.S. solar photovoltaic supply chain”, 2023 Environ. Res. Lett. 18 104012, doi: 10.1088/1748-9326/acf50d
[29] R. Besseau, « INCER ACV - Impacts environnementaux de la filière photovoltaïque & évaluation des incertitudes ». Consulté le: 7 décembre 2022. [En ligne]. Disponible sur: http://viewer.webservice-energy.org/incer-acv/app/
[30] Vidal O, Le Boulzec H, Andrieu B, Verzier F. Modelling the Demand and Access of Mineral Resources in a Changing World. Sustainability. 2022; 14(1):11. https://doi.org/10.3390/su14010011
[31] Besseau R, Tannous S, Douziech M, et al. An open-source parameterized life cycle model to assess the environmental performance of silicon-based photovoltaic systems. Prog Photovolt Res Appl. 2023; 31(9): 908-920. doi:10.1002/pip.3695
[32] Romain Besseau, Romain Sacchi, Isabelle Blanc, Paula Pérez-López, Past, present and future environmental footprint of the Danish wind turbine fleet with LCA_WIND_DK, an online interactive platform, Renewable and Sustainable Energy Reviews, Volume 108, 2019, Pages 274-288, ISSN 1364-0321, https://doi.org/10.1016/j.rser.2019.03.030.
[33] Jinyan Wang, Xiuzhi Chen, Zhongwei Liu, Veronica F. Frans, Zhenci Xu, Xinjiao Qiu, Feipeng Xu, Yunkai Li, Assessing the water and carbon footprint of hydropower stations at a national scale, Science of The Total Environment, Volume 676,2019, Pages 595-612, ISSN 0048-9697, https://doi.org/10.1016/j.scitotenv.2019.04.148.
[34] Upendra M. Sainju, Brett L. Allen, Carbon footprint of perennial bioenergy crop production receiving various nitrogen fertilization rates,Science of The Total Environment, Volume 861,2023,160663, ISSN 0048-9697, https://doi.org/10.1016/j.scitotenv.2022.160663.
[35] Yian Zhu, Siqi Wu, Jiayi Li, Qi Jia, Tiantian Zhang, Xuedan Zhang, Dongliang Han, Yufei Tan,Towards a carbon-neutral community: Integrated renewable energy systems (IRES)–sources, storage, optimization, challenges, strategies and opportunities, Journal of Energy Storage, Volume 83, 2024, 110663, ISSN 2352-152X, https://doi.org/10.1016/j.est.2024.110663.

[36] Anupam Parlikar, Benedikt Tepe, Marc Möller, Holger Hesse, Andreas Jossen, Quantifying the carbon footprint of energy storage applications with an energy system simulation framework — Energy System Network, Energy Conversion and Management, Volume 304, 2024, 118208, ISSN 0196-8904, https://doi.org/10.1016/j.enconman.2024.118208.
[37] A. Parlikar, C. N. Truong, A. Jossen, et H. Hesse, « The carbon footprint of island grids with lithium-ion battery systems: An analysis based on levelized emissions of energy supply », Renew. Sustain. Energy Rev., vol. 149, p. 111353, oct. 2021, doi: 10.1016/j.rser.2021.111353.
[38] P. Sandwell et al., « Off-grid solar photovoltaic systems for rural electrification and emissions mitigation in India », Sol. Energy Mater. Sol. Cells, vol. 156, p. 147156, nov. 2016, doi: 10.1016/j.solmat.2016.04.030.
[39] G. Falchetta, « Harnessing finance for a new era of decentralised electricity access: A review of private investment patterns and emerging business models », Soc. Sci., p. 15, 2022.
[40] C. Breyer, O. Koskinen, et P. Blechinger, « Profitable climate change mitigation: The case of greenhouse gas emission reduction benefits enabled by solar photovoltaic systems », Renew. Sustain. Energy Rev., vol. 49, p. 610628, sept. 2015, doi: 10.1016/j.rser.2015.04.061.
[41] D. Baldi, M. Moner-Girona, E. Fumagalli, et F. Fahl, « Planning sustainable electricity solutions for refugee settlements in sub-Saharan Africa », Nat. Energy, vol. 7, no 4, Art. no 4, avr. 2022, doi: 10.1038/s41560-022-01006-9.
[42] N. Rangel, H. Li, et P. Aristidou, « An optimisation tool for minimising fuel consumption, costs and emissions from Diesel-PV-Battery hybrid microgrids », Appl. Energy, vol. 335, p. 120748, avr. 2023, doi: 10.1016/j.apenergy.2023.120748.
[43] M. R. Elkadeem, A. Younes, S. W. Sharshir, P. E. Campana, et S. Wang, « Sustainable siting and design optimization of hybrid renewable energy system: A geospatial multi-criteria analysis », Appl. Energy, vol. 295, p. 117071, août 2021, doi: 10.1016/j.apenergy.2021.117071.
[44] Y. Faydi, A. Djdiaa, H. Laabassi, A. Ait Omar, et H. Bouzekri, « Contribution of green hydrogen vector to guarantee electricity feeding in remote areas- Case study », Renew. Energy, vol. 222, p. 119880, févr. 2024, doi: 10.1016/j.renene.2023.119880.
[45] N. Stevanato et al., « Planning third generation minigrids: Multi-objective optimization and brownfield investment approaches in modelling village-scale on-grid and off-grid energy systems », Renew. Sustain. Energy Transit., vol. 3, p. 100053, août 2023, doi: 10.1016/j.rset.2023.100053.
[46] M. R. Basir Khan, R. Jidin, J. Pasupuleti, et S. A. Shaaya, « Optimal combination of solar, wind, micro-hydro and diesel systems based on actual seasonal load profiles for a resort island in the South China Sea », Energy, vol. 82, p. 8097, mars 2015, doi: 10.1016/j.energy.2014.12.072.
[47] M. T. Castro, L. L. Delina, E. A. Esparcia, et J. D. Ocon, « Storm hardening and insuring energy systems in typhoon-prone regions: A techno-economic analysis of hybrid renewable energy systems in the Philippines' Busuanga island cluster », Energy Strategy Rev., vol. 50, p. 101188, nov. 2023, doi: 10.1016/j.esr.2023.101188.
[48] A. Chaurey et T. C. Kandpal, « Carbon abatement potential of solar home systems in India and their cost reduction due to carbon finance », Energy Policy, vol. 37, no 1, p. 115125, janv. 2009, doi: 10.1016/j.enpol.2008.07.038.
[49] O. D. T. Odou, « Hybrid off-grid renewable power system for sustainable rural electrification in Benin », Renew. Energy, p. 14, 2020.
[50] P. Ortega-Arriaga, O. Babacan, J. Nelson, et A. Gambhir, « Grid versus off-grid electricity access options: A review on the economic and environmental impacts », Renew. Sustain. Energy Rev., vol. 143, p. 110864, juin 2021, doi: 10.1016/j.rser.2021.110864.
[51] Y. Tsuchiya, T. A. Swai, et F. Goto, « Energy payback time analysis and return on investment of off-grid photovoltaic systems in rural areas of Tanzania », Sustain. Energy Technol. Assess., vol. 42, p. 100887, déc. 2020, doi: 10.1016/j.seta.2020.100887.
[52] E. Tsiaras, D. N. Papadopoulos, C. N. Antonopoulos, V. G. Papadakis, et F. A. Coutelieris, « Planning and assessment of an off-grid power supply system for small settlements », Renew. Energy, vol. 149, p. 12711281, avr. 2020, doi: 10.1016/j.renene.2019.10.118.

[53] H. Beath, J. Baranda Alonso, R. Mori, A. Gambhir, J. Nelson, et P. Sandwell, « Maximising the benefits of renewable energy infrastructure in displacement settings: Optimising the operation of a solar-hybrid mini-grid for institutional and business users in Mahama Refugee Camp, Rwanda », Renew. Sustain. Energy Rev., vol. 176, p. 113142, avr. 2023, doi: 10.1016/j.rser.2022.113142.
[54] M. Gandiglio, P. Marocco, I. Bianco, D. Lovera, G.A. Blengini, M. Santarelli, Life cycle assessment of a renewable energy system with hydrogen-battery storage for a remote off-grid community, International Journal of Hydrogen Energy, Volume 47, Issue 77, 2022, Pages 32822-32834, ISSN 0360-3199, https://doi.org/10.1016/j.ijhydene.2022.07.199.
[55] Christopher S. McCallum, Narendran Kumar, Robin Curry, Katherine McBride, John Doran, Renewable electricity generation for off grid remote communities; Life Cycle Assessment Study in Alaska, USA, Applied Energy, Volume 299, 2021, 117325, ISSN 0306-2619, https://doi.org/10.1016/j.apenergy.2021.117325.
[56] Iván Jiménez-Vargas, Juan M. Rey, German Osma-Pinto, Sizing of hybrid microgrids considering life cycle assessment, Renewable Energy, Volume 202, 2023, Pages 554-565, ISSN 0960-1481, https://doi.org/10.1016/j.renene.2022.11.103.
[57] F. Antonanzas-Torres, J. Antonanzas, et J. Blanco-Fernandez, « Environmental life cycle impact of off-grid rural electrification with mini grids in West Africa », Sustain. Energy Technol. Assess., vol. 47, p. 101471, oct. 2021, doi: 10.1016/j.seta.2021.101471.
[58] LU, Jiaqi, TANG, Jing, SHAN, Rui, et al. Spatiotemporal analysis of the future carbon footprint of solar electricity in the United States by a dynamic life cycle assessment. Iscience, 2023, vol. 26, no 3.
[59] M. Thirunavukkarasu, Yashwant Sawle, Himadri Lala, A comprehensive review on optimization of hybrid renewable energy systems using various optimization techniques, Renewable and Sustainable Energy Reviews, Volume 176, 2023, 113192, ISSN 1364-0321, https://doi.org/10.1016/j.rser.2023.113192.
[60] Yi He, Su Guo, Peixin Dong, Yi Zhang, Jing Huang, Jianxu Zhou, A state-of-the-art review and bibliometric analysis on the sizing optimization of off-grid hybrid renewable energy systems, Renewable and Sustainable Energy Reviews, Volume 183, 2023, 113476, ISSN 1364-0321, https://doi.org/10.1016/j.rser.2023.113476.
[61] A. Boadzo, S. K. Kibaara, et S. Chowdhury, « A study on dairy farm-based hybrid renewable energy systems in South Africa », p. 5.
[62] S. Gabra, J. Miles, et S. A. Scott, « Techno-economic analysis of stand-alone wind micro-grids, compared with PV and diesel in Africa », Renew. Energy, vol. 143, p. 19281938, déc. 2019, doi: 10.1016/j.renene.2019.05.119.
[63] Dwipen Boruah, Shyam Singh Chandel, Techno-economic feasibility analysis of a commercial grid-connected photovoltaic plant with battery energy storage-achieving a net zero energy system, Journal of Energy Storage, Volume 77, 2024, 109984, ISSN 2352-152X, https://doi.org/10.1016/j.est.2023.109984.
[64] Ijeoma MW, Chen H, Carbajales-Dale M, Yakubu RO. Techno-Economic Assessment of the Viability of Commercial Solar PV System in Port Harcourt, Rivers State, Nigeria. Energies. 2023; 16(19):6803. https://doi.org/10.3390/en16196803
[65] Rehmani AM, Kazmi SAA, Altamimi A, Khan ZA, Awais M. Techno-Economic-Environmental Assessment of an Isolated Rural Micro-Grid from a Mid-Career Repowering Perspective. Sustainability. 2023; 15(3):2137. https://doi.org/10.3390/su15032137
[66] F. F. Nerini, O. Broad, D. Mentis, M. Welsch, M. Bazilian, et M. Howells, « A cost comparison of technology approaches for improving access to electricity services », Energy, vol. 95, p. 255265, janv. 2016, doi: 10.1016/j.energy.2015.11.068.
[67] M. Moner-Girona et al., « Decentralized rural electrification in Kenya: Speeding up universal energy access », Energy Sustain. Dev., vol. 52, p. 128146, oct. 2019, doi: 10.1016/j.esd.2019.07.009.

[68] Emília Inês Come Zebra, Henny J. van der Windt, Geraldo Nhumaio, André P.C. Faaij, A review of hybrid renewable energy systems in mini-grids for off-grid electrification in developing countries, Renewable and Sustainable Energy Reviews, Volume 144, 2021, 111036, ISSN 1364-0321, https://doi.org/10.1016/j.rser.2021.111036.
[69] A. K. Stinder, S. Finke, M. Vendeleric, et S. Severengiz, « A generic GHG-LCA model of a smart mini grid for decision making using the example of the Don Bosco mini grid in Tema, Ghana », Procedia CIRP, vol. 105, p. 776781, janv. 2022, doi: 10.1016/j.procir.2022.02.129.
[70] M. Bortolini, M. Gamberi, A. Graziani, et F. Pilati, « Economic and environmental bi-objective design of an off-grid photovoltaic–battery–diesel generator hybrid energy system », Energy Convers. Manag., vol. 106, p. 10241038, déc. 2015, doi: 10.1016/j.enconman.2015.10.051.
[71] N. Plain, B. Hingray, et S. Mathy, « Accounting for low solar resource days to size 100% solar microgrids power systems in Africa », Renew. Energy, vol. 131, p. 448458, févr. 2019, doi: 10.1016/j.renene.2018.07.036.
[72] Seyedhashemi H, Hingray B, Lavaysse C, Chamarande T. The Impact of Low-Resource Periods on the Reliability of Wind Power Systems for Rural Electrification in Africa. Energies. 2021; 14(11):2978. https://doi.org/10.3390/en14112978
[73] Isabelle Viole, Guillermo Valenzuela-Venegas, Sabrina Sartori, Marianne Zeyringer, Integrated life cycle assessment in off-grid energy system design—Uncovering low hanging fruit for climate mitigation, Applied Energy, Volume 367, 2024, 123334, ISSN 0306-2619, https://doi.org/10.1016/j.apenergy.2024.123334.
[74] T. Chamarande, S. Mathy, et B. Hingray, « The least cost design of 100 % solar power microgrids in Africa: Sensitivity to meteorological and economic drivers and possibility for simple pre-sizing rules », Energy Sustain. Dev., vol. 69, p. 211223, août 2022, doi: 10.1016/j.esd.2022.07.001.
[75] Tom Terlouw, Paolo Gabrielli, Tarek AlSkaif, Christian Bauer, Russell McKenna, Marco Mazzotti, Optimal economic and environmental design of multi-energy systems, Applied Energy, Volume 347, 2023, 121374, ISSN 0306-2619, https://doi.org/10.1016/j.apenergy.2023.121374.
[76] Phantisa Limleamthong, Gonzalo Guillén-Gosálbez, Rigorous analysis of Pareto fronts in sustainability studies based on bilevel optimization: Application to the redesign of the UK electricity mix, Journal of Cleaner Production, Volume 164, 2017, Pages 1602-1613, ISSN 0959-6526, https://doi.org/10.1016/j.jclepro.2017.06.134.
[77] Deutsche Gesellschaft für Internationale Zusammenarbeit, « International Fuel Prices 2018/19 », 2019.
[78] Bertrand Iooss, Paul Lemaître, A review on global sensitivity analysis methods, 2014, arXiv, https://doi.org/10.48550/arXiv.1404.2405
[79] V. Mukoro, M. Sharmina, et A. Gallego-Schmid, « A review of business models for access to affordable and clean energy in Africa: Do they deliver social, economic, and environmental value? », Energy Res. Soc. Sci., vol. 88, p. 102530, juin 2022, doi: 10.1016/j.erss.2022.102530.
[80] Deutsche Gesellschaft für Internationale Zusammenarbeit, « What size shall it be ? », août 2016.
[81] International Energy Agency, « IEA PVPS : Mini-réseaux hybrides PV-diesel pour l'électrification rurale », T9-13:2013, juill. 2013
[82] Ember (2024); Energy Institute - Statistical Review of World Energy (2024) – with major processing by Our World in Data. "Carbon intensity of electricity generation – Ember and Energy Institute" [dataset]. Ember, "Yearly Electricity Data"; Energy Institute, "Statistical Review of World Energy" [original data]. Retrieved July 28, 2024 from https://ourworldindata.org/grapher/carbon-intensity-electricity
[83] A. F. Crossland, O. H. Anuta, et N. S. Wade, « A socio-technical approach to increasing the battery lifetime of off-grid photovoltaic systems applied to a case study in Rwanda », Renew. Energy, vol. 83, p. 3040, nov. 2015, doi: 10.1016/j.renene.2015.04.020.
[84] C. Agutu, « Accounting for finance in electrification models for sub-Saharan Africa », Nat. EnerGy, vol. 7, p. 11, 2022.

[85] Semis et GIZ, « Livrable 2: Rapport d'état des lieux avec les données quantitatives et qualitatives sur l'état de fonctionnement de l'ensemble des ERILs et GDTs », Ministère du Pétrole et des Energies, 2020.
[86] C. André-Bataille, N. Livache, et A. Ranzanici, « Publication d'une étude de capitalisation de 16 projets d'électrification rurale à Madagascar », Fondation Energies pour le monde (FONDEM), Paris, 2020. Consulté le: 10 novembre 2022. [En ligne]. Disponible sur: https://fondem.ong/publication-dune-etude-de-capitalisation-sur-des-projets-delectrification-rurale-en-afrique/
[87] Emilie Etienne, Pierre Robert, Can isolated microgrids be viable? A longitudinal study of long-term sustainability in rural Senegal, Energy Research & Social Science, Volume 111, 2024, 103476, ISSN 2214-6296, https://doi.org/10.1016/j.erss.2024.103476.
[88] Ademola A. Adenle, Assessment of solar energy technologies in Africa-opportunities and challenges in meeting the 2030 agenda and sustainable development goals, Energy Policy, Volume 137, 2020, 111180, ISSN 0301-4215, https://doi.org/10.1016/j.enpol.2019.111180.
[89] World Bank. 2024 Guidance Note on Shadow Price of Carbon in Economic Analysis (English). Washington, D.C. : World Bank Group. http://documents.worldbank.org/curated/en/099553203142424068/IDU1c94753bb1819e14c781831215580060675b1
[90] European Investment Bank Group, « Climate Bank Roadmap 2021-2025 », nov. 2020. [En ligne]. Disponible sur: https://www.eib.org/attachments/thematic/eib_group_climate_bank_roadmap_en.pdf
[91] E. Hartvigsson et E. O. Ahlgren, « Comparison of load profiles in a mini-grid: Assessment of performance metrics using measured and interview-based data », Energy Sustain. Dev., vol. 43, p. 186195, avr. 2018, doi: 10.1016/j.esd.2018.01.009.
[92] H. Louie et P. Dauenhauer, « Effects of load estimation error on small-scale off-grid photovoltaic system design, cost and reliability », Energy Sustain. Dev., vol. 34, p. 3043, oct. 2016, doi: 10.1016/j.esd.2016.08.002.
[93] S. Mandelli, « Effect of load profile uncertainty on the optimum sizing of off-grid PV systems for rural electrification », Sustain. Energy Technol. Assess., p. 14, 2016.
[94] M. Gustavsson et D. Mtonga, « Lead-acid battery capacity in solar home systems—Field tests and experiences in Lundazi, Zambia », Sol. Energy, vol. 79, no 5, Art. no 5, nov. 2005, doi: 10.1016/j.solener.2004.10.010.
[95] International Energy Agency, « Africa Energy Outlook 2019 ». [En ligne]. Disponible sur: https://www.iea.org/reports/africa-energy-outlook-2019
[96] Climate Watch et World Resource Institute, « Data Explorer | Climate Watch ». Consulté le: 28 février 2023. [En ligne]. Disponible sur: https://www.climatewatchdata.org/data-explorer/historical-emissions
[97] Oyelami, S., Okedere, O. B., Oyewole, K. A., Rabiu, K. O., Alamu, O. J., Sulaimon, M. D., & Lawal, S. O. (2023). Impact of diesel fuel generators on soil heavy metals. Journal of Engineering Studies and Research, 29(1), 54-60. Retrieved from https://jesr.ub.ro/1/article/view/371
[98] Hosseinzadeh-Bandbafha, H., Rafiee, S., Mohammadi, P., Ghobadian, B., Lam, S. S., Tabatabaei, M., & Aghbashlo, M. (2021). Exergetic, economic, and environmental life cycle assessment analyses of a heavy-duty tractor diesel engine fueled with diesel–biodiesel-bioethanol blends. Energy Conversion and Management, 241, 114300. doi:10.1016/j.enconman.2021.114300
[99] Badza, K., Soro, Y.M. & Sawadogo, M. Photovoltaic waste management in sub-Saharan Africa: current practices in Burkina Faso. Waste Dispos. Sustain. Energy 6, 271–282 (2024). https://doi.org/10.1007/s42768-023-00184-w
[100] U. Pfeifroth et al., « Surface Radiation Data Set - Heliosat (SARAH) - Edition 2 ». Satellite Application Facility on Climate Monitoring (CM SAF), 13 juin 2017. doi: 10.5676/EUM_SAF_CM/SARAH/V002.

[101] Hersbach H, Bell B, Berrisford P, et al. The ERA5 global reanalysis. Q J R Meteorol Soc. 2020; 146: 1999–2049. https://doi.org/10.1002/qj.3803
[102] E. L. Maxwell, « A Quasi-Physical Model for Converting Hourly Global Horizontal to Direct Normal lnsolation », Solar Energy Research Institute, Midwest Research Institute, août 1987.
[103] A. Bahrami, « The effect of latitude on the performance of different solar trackers in Europe and Africa », Appl. Energy, p. 11, 2016.
[104] E. Lorenz, T. Scheidsteger, J. Hurka, D. Heinemann, et C. Kurz, « Regional PV power prediction for improved grid integration », p. 15, 2010.
[105] H. Louie, Off-grid electrical systems in developing countries. New York, NY: Springer Science+Business Media, 2018.
[106] T. Huld, M. Moner-Girona, et A. Kriston, « Geospatial Analysis of Photovoltaic Mini-Grid System Performance », Energies, vol. 10, no 2, Art. no 2, févr. 2017, doi: 10.3390/en10020218.
[107] S. Mandelli, C. Brivio, M. Moncecchi, F. Riva, G. Bonamini, et M. Merlo, « Novel LoadProGen procedure for micro-grid design in emerging country scenarios: application to energy storage sizing », Energy Procedia, vol. 135, p. 367378, oct. 2017, doi: 10.1016/j.egypro.2017.09.528.
[108] X. Li, J. Salasovich, et T. Reber, « Microgrid Load and LCOE Modelling Results ». National Renewable Energy Laboratory, 2018. [En ligne]. Disponible sur: https://data.nrel.gov/submissions/79
[109] N. J. Williams, P. Jaramillo, B. Cornell, I. Lyons-Galante, et E. Wynn, « Load characteristics of East African microgrids », in 2017 IEEE PES PowerAfrica, juin 2017, p. 236241. doi: 10.1109/PowerAfrica.2017.7991230.
[110] A. Stiel et M. Skyllas-Kazacos, « Feasibility Study of Energy Storage Systems in Wind/Diesel Applications Using the HOMER Model », Appl. Sci., vol. 2, no 4, Art. no 4, déc. 2012, doi: 10.3390/app2040726.
[111] G. Ayele, Renewable Energy to Support Local Development in Peru, Cusco Region. 2014. doi: 10.13140/RG.2.2.30621.77280.
[112] IRENA, « The Power to Change: Solar and Wind Cost Reduction Potential to 2025 », 2016.
[113] IRENA, « Electricity storage and renewables: Costs and markets to 2030 », 2017.
[114] IRENA, « Solar PV in Africa : costs and markets », IRENA, sept. 2016. Consulté le: 2 décembre 2021. [En ligne]. Disponible sur: https://www.irena.org/-/media/Files/IRENA/Agency/Publication/2016/IRENA_Solar_PV_Costs_Africa_2016.pdf